
Masters Theses

Student Theses and Dissertations

Fall 2014

The effects of advanced structural materials to mitigate explosive and impact threats

Caleb Michael Baumgart

Follow this and additional works at: https://scholarsmine.mst.edu/masters_theses



Part of the [Explosives Engineering Commons](#)

Department:

Recommended Citation

Baumgart, Caleb Michael, "The effects of advanced structural materials to mitigate explosive and impact threats" (2014). *Masters Theses*. 7320.

https://scholarsmine.mst.edu/masters_theses/7320

This thesis is brought to you by Scholars' Mine, a service of the Missouri S&T Library and Learning Resources. This work is protected by U. S. Copyright Law. Unauthorized use including reproduction for redistribution requires the permission of the copyright holder. For more information, please contact scholarsmine@mst.edu.

THE EFFECTS OF ADVANCED STRUCTURAL MATERIALS TO
MITIGATE EXPLOSIVE AND IMPACT THREATS

By

CALEB MICHAEL BAUMGART

A THESIS

Presented to the Faculty of the Graduate School of the
MISSOURI UNIVERSITY OF SCIENCE AND TECHNOLOGY

In Partial Fulfillment of the Requirements for the Degree

MASTER OF SCIENCE

IN

EXPLOSIVES ENGINEERING

2014

Approved by:

Jason Baird
Paul Worsey
John J. Myers

© 2014

CALEB MICHAEL BAUMGART

ALL RIGHTS RESERVED

ABSTRACT

In a world of ever newer and modified improvised explosive devices (IEDs) that are very common in certain parts of the world, it is always more important to improve the devices used for protection. This research endeavors to design and analyze a blast barrier using three different media types to mitigate the high pressures from an IED or a car bomb. The three media types used in this research are pumice, steel grit, and foam. Six barriers were built to test the three media types and account for the changes from a standard solid concrete barrier to a barrier with a cavity and media. The different media were tested for peak overpressure and impulse reduction. Test panels were subjected to various standoff distances and three charges were tested at each standoff distance. Of the three different media types tested steel grit showed the largest reduction in peak overpressure and impulse. It is the hope of the author that this research will take the first steps in designing a new blast mitigating barrier that is easily built and deployed to better protect buildings and save lives.

ACKNOWLEDGMENTS

I would first and foremost like to offer my deepest gratitude to Dr. Jason Baird, who gave me the opportunity to better myself and discover my capabilities. Without his help, patience and direction, that always kept me thinking, this work would never have been done. I thank Dr. Paul Worsley and his wife Dr. Gill Worsley for their sharing of knowledge and keeping me on track to reach my goal. I thank Dr. John Myers for the help in construction and knowledge that was shared. I would like to thank Ish Keener and his company ProPerma for all their help and donating the long carbon fibers used in this research. I thank Jimmie Taylor, Sr. and Dewayne Phelps for their help at the mine and keeping the mine open past the normal hours of operation so I could get my research done. I would also like to thank Randy Forchee, John Bullock, Benjamin Gliha, Julie Willey, Jerry Vaill, David Phelps, Benjamin Anderson, Barbara Robertson, Shirley Hall and Judy Russell for their assistance throughout all of my research.

I would like to give a special thanks to Phillip Mulligan and Kevin Phelps for allowing me to use their knowledge, experience and the many hours of help given to me during testing. This research would not have been accomplished in a timely manner nor been as robust without their help. I would like to thank all of my friends and family for their encouragement and support and for always believing in me.

TABLE OF CONTENTS

	Page
ABSTRACT.....	iii
ACKNOWLEDGMENTS.....	iv
LIST OF ILLUSTRATIONS.....	viii
LIST OF TABLES.....	x
NOMENCLATURE.....	xi
 SECTION	
1. INTRODUCTION.....	1
2. LITERATURE REVIEW.....	3
2.1 THE MITIGATION EFFECTS OF A BARRIER WALL ON BLAST WAVE PRESSURES (ROUSE, 2010).....	3
2.2 INVESTIGATION OF A HIGH-VOLUME FLY ASH-WOOD FIBER MATERIAL SUBJECTED TO LOW-VELOCITY IMPACT AND BLAST LOADS (TINSLEY ET. AL., 2007).....	7
2.3 PREDICTION OF AIRBLAST LOADS ON STRUCTURES BEHIND A PROTECTIVE BARRIER (ZHOU ET. AL., 2007).....	8
2.4 DUCTAL [®] – AN ULTRA-HIGH PERFORMANCE MATERIAL FOR RESISTANCE TO BLASTS AND IMPACTS (CAVILL ET. AL., 2006).....	11
2.5 ENERGY TRAPPING AND SHOCK DISINTEGRATION IN A COMPOSITE GRANULAR MEDIUM (DARAIO ET. AL., 2006).....	16
2.6 SHOCK (BLAST) MITIGATION BY “SOFT” CONDENSED MATTER (NESTERENKO, 2003).....	18
2.7 SCIENTIFIC PRINCIPLES (BREWER, 1999).....	22
3. BLAST BARRIER DESIGN.....	23

3.1	CONCRETE.....	23
3.2	LONG CARBON FIBER REINFORCEMENT.....	26
3.3	CONSTRUCTION.....	31
3.4	DESIGN.....	32
4.	EXPLOSIVE PROPERTIES.....	36
4.1	BEC.....	41
4.2	MEDIA SELECTION.....	42
4.2.1	Pumice.....	43
4.2.2	Steel Grit.....	44
4.2.3	Foam.....	44
5.	TESTING METHODS.....	47
6.	DATA ANALYSIS.....	57
7.	CONCLUSIONS.....	67
8.	FUTURE WORK.....	68
APPENDICES		
A.	CONCRETE FORMULA SHEET.....	69
B.	MATLAB CODE FOR EXPLOSION PROPERTIES.....	71
C.	TRANSDUCER SPECIFICATION SHEET.....	80
D.	TEST SETUP MATRIX.....	82
E.	STEP-BY-STEP PROCESS TO CALIBRATE DAS.....	84
F.	WEATHER CONDITIONS FOR TEST DAYS.....	93
G.	STEP-BY-STEP PROCESS TO CALCULATE IMPULSE.....	95
H.	TEST VALUES.....	102

I. PICTURES.....	104
BIBLIOGRAPHY.....	108
VITA.....	110

LIST OF ILLUSTRATIONS

	Page
Figure 2.1 Blast table with charge and pressure recording locations (Rouse, 2010).....	4
Figure 2.2 Blast wave diffraction over a barrier (Rouse, 2010).....	5
Figure 2.3 Percent reduction contour chart (Rouse, 2010).....	6
Figure 2.4 Geometric relationship between the wall height, standoff distance, and location of the pressure reduction boundary (Rouse, 2010).....	7
Figure 2.5 Blast layout configuration (Zhou et. al., 2007).....	11
Figure 2.6 Typical force deformation response of Ductal [®] in compression and flexure (Cavill et.al., 2006).....	13
Figure 2.7 Test panels 3 and 4 after close charge explosion (Cavill et.al., 2006).....	15
Figure 2.8 Pulse trapping in the composite granular protector with two PTFE sections (Daraio et.al., 2006).....	17
Figure 2.9 Three types of impulse loading P(t): (a) triangular pulse with sharp front and duration $t_1 \ll T$, (b) step function with sharp increase of pressure and (c) ramp function with finite time τ of pressure increase. P(t) represents pressure in a reflected shock wave(Nesterenko, 2003).....	19
Figure 2.10 (a) Catastrophic failure of steel structure after inside explosion in air and (b) confined explosion in the same structure filled with sawdust. Explosive (RDX) mass was 0.5 kg in both cases, wall thickness of containers 3 mm, side 0.7 m, sawdust density 100 kg/m ³ (Nesterenko, 2003).....	21
Figure 3.1 Slump test on concrete.....	25
Figure 3.2 Compression strength test plot.....	26
Figure 3.3 Mixing the LCFs by hand.....	27
Figure 3.4 Long carbon fibers (Properma, 2014).....	29
Figure 3.5 Foam cutout dimensions.....	33
Figure 3.6 Construction of foam filler and framework.....	34
Figure 3.7 Frame and foam secured and ready for pour.....	35

Figure 4.1 Pressure curve from a blast wave (Chaurasia, 2011).....	36
Figure 4.2 Pressure wave from low impedance to high impedance (Cooper, 1997)	38
Figure 4.3 Pressure wave from high impedance to low impedance (Cooper, 1997).....	40
Figure 4.4 2-mm pumice.....	43
Figure 4.5 2-mm steel grit.....	44
Figure 4.6 Canister and foam sprayed on board to observe expansion.....	45
Figure 5.1 Pressure transducer 102B15.....	48
Figure 5.2 Synergy DAS computer.....	49
Figure 5.3 Underground test facility layout.....	51
Figure 5.4 Experimental test layout	53
Figure 5.5 Aboveground test site	54
Figure 6.1 Barrier chained to supporting I-beams.....	59
Figure 6.2 Side of barrier with cavity.....	60
Figure 6.3 Front face of barrier with cavity.....	61
Figure 6.4 Normalized impulses at distance 0.3 m, showing percent impulse difference between the barrier and barrier 1.....	62
Figure 6.5 Normalized impulses at distance 0.6 m, showing percent impulse difference between the barrier and barrier 1.....	63
Figure 6.6 Normalized impulses at distance 1.5 m, showing percent impulse difference between the barrier and barrier 1.....	63
Figure 6.7 Normalized pressure at distance 0.3 m, showing percent pressure difference between the barrier and barrier 1.....	64
Figure 6.8 Normalized pressure at distance 0.6 m, showing percent pressure difference between the barrier and barrier 1.....	64
Figure 6.9 Normalized pressure at distance 1.5 m, showing percent pressure difference between the barrier and barrier 1.....	65

LIST OF TABLES

	Page
Table 2.1 Main observations, Woomera blast trial (Cavill et.al., 2006).....	14
Table 2.2 Panel details for close charge tests (Cavill et.al., 2006).....	15
Table 3.1 Carbon Fiber Properties (Volz et.al., 2010).....	28
Table 3.2 Fiber properties used in this research (Properma, 2014).....	30
Table 5.1 BEC approximation table of expected test values.....	48
Table 6.1 Barrier configuration.....	59
Table 6.2 Damage to barriers during testin.....	60

NOMENCLATURE

Symbol	Description
A	Area
A_I	Impulse modification factor
A_P	Pressure modification factor
b	Decay coefficient
B1	Barrier 1, Solid concrete
B2	Barrier 2, Hollow cavity
B3	Barrier 3, Hollow cavity with Long carbon fiber
B4	Barrier 4, Foam
B5	Barrier 5, Pumice
B6	Barrier 6, Steel grit
BEC	Blast effects computer
CMOS	Complementary metal oxide silicon
C_o	Bulk sound speed
D	Distance from charge to building
DAS	Digital acquisition system
DDESD	Department of Defense Explosives Safety Board
F	Degrees Fahrenheit
ft/lb^3	Feet per pound cubed
g	Grams
H^*	Critical thickness of damping material

H_1	Blast wall height
H_e	Vertical distance on building
H_z	Hertz
I	Impulse
IED	Improvised explosive device
$I_{no_barrier}$	Impulse without a barrier
$I_{with_barrier}$	Impulse with a barrier
kg	Kilograms
kg/m^3	Kilogram/meter cubed
kg/m	Kilograms per meter
kPa	Kilopascals
L_1	Distance between charge and barrier (standoff distance)
LCF	Long carbon fiber
lg	Log base 10
m	Meters
mbar	Millibars
mm	Millimeters
MPa	Megapascals
ms	Miliseconds
MS/s	Megasample per second
m/s	Meters per second
mV	Millivolts
N.E.W.	Net equivalent weight

oz	Ounces
P	Pressure
$P_{\text{no_barrier}}$	Pressure with no barrier
P_o or P_a	Ambient pressure
P_s	Peak pressure
psi	Pounds per square inch
PVC	Polyvinyl chloride
$P_{\text{with_barrier}}$	Pressure with barrier
RPC	Reactive powder concrete
s	Seconds
S	Empirical constant for a given material
SLR	Single-lens reflex
T^+	Positive phase
t	Time
T_a	Time of arrival
u_1	Particle velocity after the shock
u	Particle velocity
V	Volts
VOD	Velocity of detonation
W	Charge weight
Z	Scaled distance
ρ_o	Density
μsec	Microseconds

1. INTRODUCTION

The author is a student of the Missouri University of Science and Technology (Missouri S&T) Mining & Nuclear Engineering Department, which administers the Explosive Engineering program. This research started in conjunction with several other universities under the U.S. Department of Homeland Security (DHS) ALERT F4E project. The University of Rhode Island (URI) was the thrust leader for the blast mitigation, so the research for the project began in conjunction with URI and under its leadership. Before completing the research, the DHS fiscal year ended with no funding extension given, so Missouri S&T funded the remainder of the project.

This research is meant to expound and extrapolate on research previously done on "soft" condensed matter to mitigate shock from an explosive charge (Nesterenko, 2003). In order to achieve the goal for this research two main questions are addressed herein. Can a proven blast mitigating material placed inside a barrier at a given standoff distance still mitigate energy from a blast wave? In addition, are there other mitigating materials that work better compared with materials already in use?

For this project a method was needed to test the different media. A nonstandard concrete barrier designed with a hollow cavity gives the ability to fill that cavity with different media and test those media. The construction of all barriers made use of the many necessary forms and tools in the Butler-Carlton High-bay on the Missouri S&T campus. All testing for this project was conducted at Missouri S&T's Experimental Mine. The testing made use of two sites on the mine facility; an aboveground test site and a belowground test site. Both sites, used for different advantages, were needed to complete the project. The underground site provides steady temperatures and the ability to use

larger explosive charges (a maximum of 7.7 kg). The aboveground site provides a larger test site that is not confined and video capabilities are possible due to brightness. The maximum explosive charge size is 0.9 kg for the aboveground site.

2. LITERATURE REVIEW

In order to provide new reliable research a thorough literature review was done. This research encompasses many subject areas including, but not limited to, concrete, explosives, shock wave propagation, and blast mitigation. Google searches, Missouri S&T's library, and several online journals were used as sources for the literary review. This literature was used to provide insight into concrete, shock wave mitigation, shock wave reflection, energy absorption and calculating blast parameters behind a blast wall. The following is a review of the literature most used in this research, in order by publication date from most current to the most dated.

2.1 THE MITIGATION EFFECTS OF A BARRIER WALL ON BLAST WAVE PRESSURES (ROUSE, 2010)

The most recent research found is by Nathan Rouse, who looked into the effects a barrier has on blast wave pressures. This research, done at Missouri S&T's Experimental Mine, uses a blast table to coordinate an array of pressure transducers in a way that allows the user to map the pressure behind a barrier or blast wall. In order to accomplish this research on a table the author scaled down all actual charge weights and distances by a factor of 50. This scale allowed the author to use much smaller hemispherical charges of Composition-4 (C-4). A charge was placed at each of three different standoff distances from the barrier. This allowed Rouse to determine if the placement and wall height of a barrier from an explosive are more beneficial than the distance without a barrier. Three wall heights were used in order to test the barriers effectiveness. To obtain an accurate map on the backside of the barrier, 45 pressure transducers were mounted from

underneath the table. The face of each pressure transducer is threaded into a tapped hole until it is flush with the top of the table. Making the transducers flush with the surface allows the pressure wave to move across the top of the table unaffected, getting a more accurate representation of the pressure differences. The three distances used for standoff and test setup can be seen in Figure 2.1.

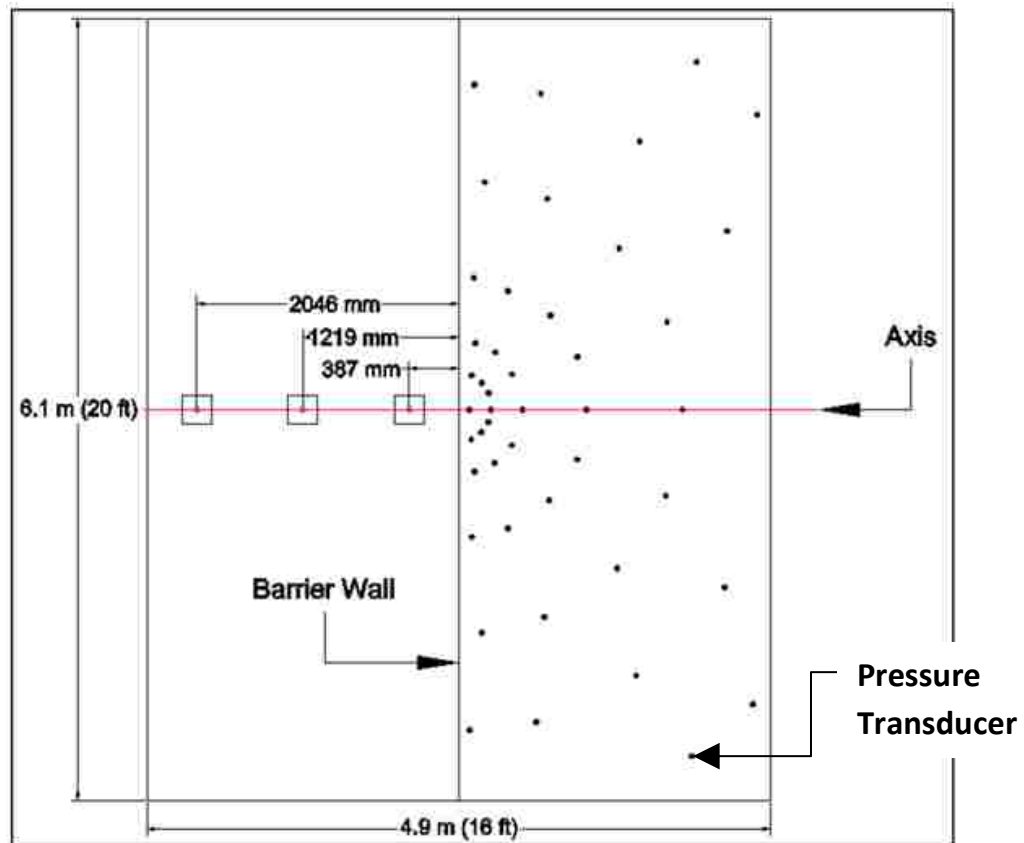


Figure 2.1 Blast table with charge and pressure recording locations (Rouse, 2010)

To help understand why the pressures map the way they do, a better understanding of how a blast wave propagates is needed. According to the thesis, three

things happen when a blast wave encounters an object. The blast wave is reflected, absorbed, and transmitted by that object. When a barrier exists, part of the blast wave is reflected back from the way it came as well as wrapping around the top of the barrier. The majority of the blast wave in most cases is reflected around or over the barrier as shown in Figure 2.2, and not absorbed nor transmitted.

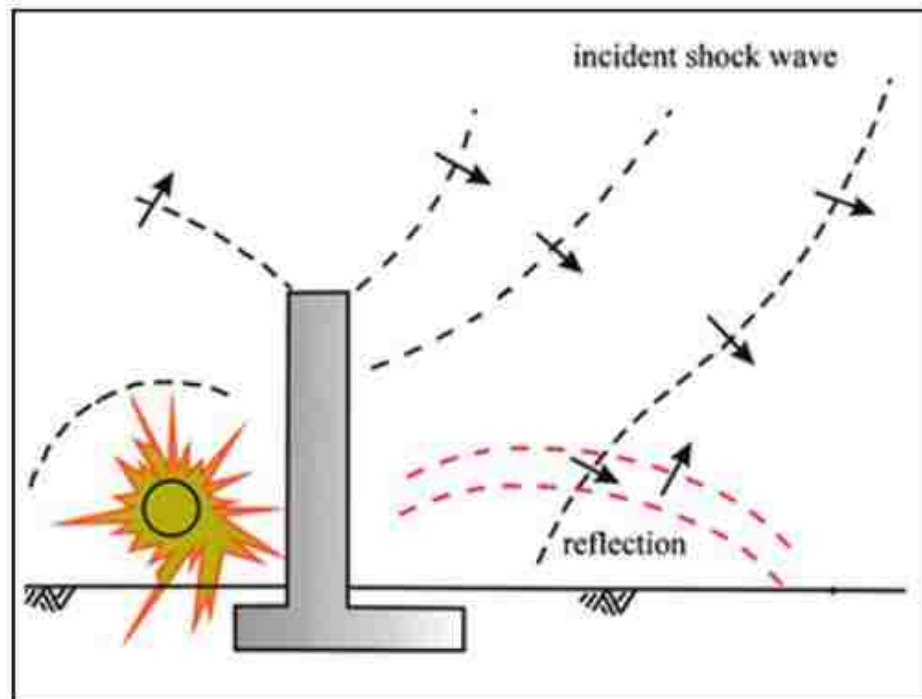


Figure 2.2 Blast wave diffraction over a barrier (Rouse, 2010)

This research made use of a Synergy digital acquisition system (DAS) to record the data from the pressure transducers. Several explosive charges were shot at each position in order to average the data. In order to not damage the table charges are set on cardboard squares which are then set into square cutouts in the table. Once the values

were averaged, the data was fed into a Matlab program created by Rouse. This Matlab program takes the values inserted into it and creates a plot of the pressures. A sample of the pressure distribution is shown in Figure 2.3. The distance along the barrier is on the y-axis, in mm, and the distance away from the barrier is on the x-axis in mm. The pressure differences are represented by color on the right side of the graph, with dark blue being atmospheric pressure and dark red maximum pressure created by the explosive charge.

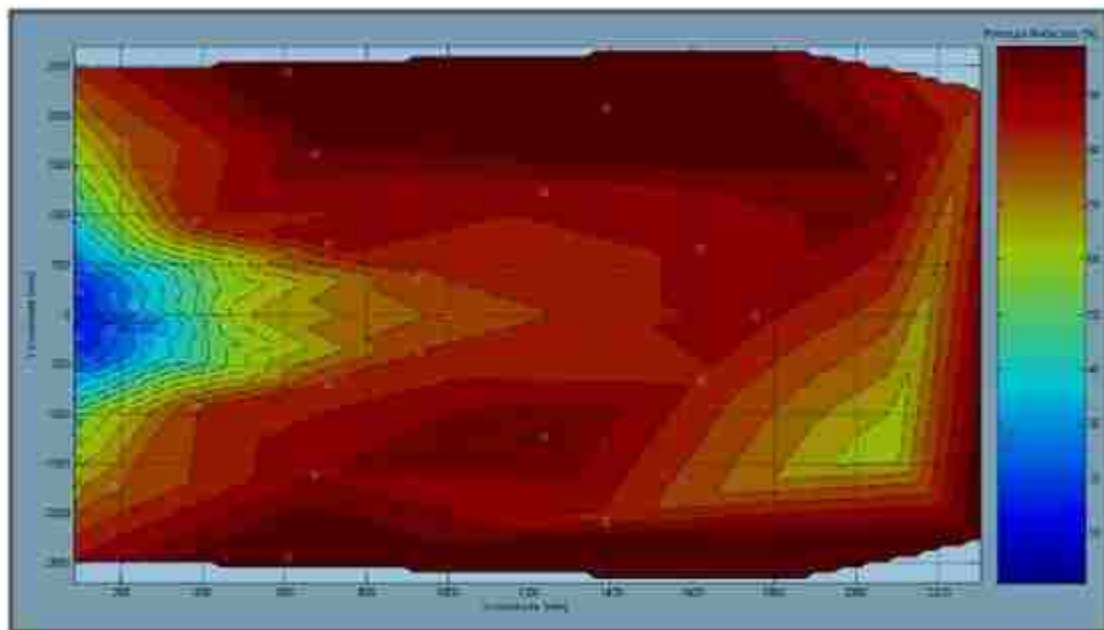


Figure 2.3 Percent reduction contour chart (Rouse, 2010)

In his conclusions, Rouse found that there is a nonlinear relationship between the angle created from the charge to the top of the wall and the angle on the backside of the barrier from the top of the wall to the ground. See Figure 2.4.

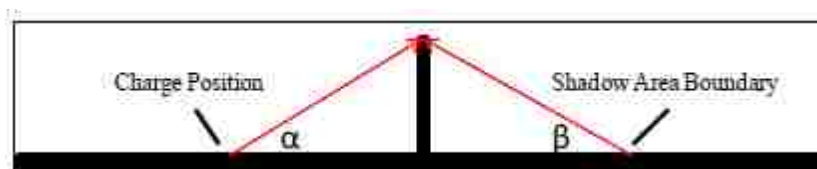


Figure 2.4 Geometric relationship between the wall height, standoff distance, and location of the pressure reduction boundary (Rouse, 2010).

This relationship can be used to predict how large the shadow region will be on the backside of the wall. The shadow region is an area behind the barrier where the pressure is significantly reduced. It is also proven in Rouse's paper that to achieve lower pressures behind the barrier it is better to have a larger standoff distance than to have a higher wall. However, increasing the wall height affects the shadow region, up to ten times more than increasing the standoff distance. This is because of the laws of sound propagation, which state, the pressure drops by a factor of ten when the distance from the source doubles.

2.2 INVESTIGATION OF A HIGH-VOLUME FLY ASH-WOOD FIBER MATERIAL SUBJECTED TO LOW-VELOCITY IMPACT AND BLAST LOADS (TINSLEY ET.AL., 2007)

This research by Tinsley at Missouri S&T looked at the efficiency of using high-volume fly ash-wood fiber in concrete to mitigate dynamic pressure loads. Fly ash-wood fiber is a common waste product that is an easily obtainable green material. Field tests conducted for this research showed when a modified panel is subjected to a near field blast it had improved blast resistance over plain reinforced panels. In the next series of tests, a bi-layer slab was used. The first layer of the bi-layer panel had a lower density

and was closer to the explosive charge. In a second round of testing, a polyurea coating was sprayed on the slab. This coating did not mitigate the pressure or increase the flexural strength, but it better contained the spalling and fragmenting of the concrete slab. This research helps to prove that a nonlinear composite can efficiently reduce the energy moving through the panel.

2.3 PREDICTION OF AIRBLAST LOADS ON STRUCTURES BEHIND A PROTECTIVE BARRIER (ZHOU ET.AL., 2007)

This journal article is a conglomeration of research, taking calculations done by others and combining them with Zhou's own calculations to be able to predict blast pressures and impulses behind a protective barrier. TM5-1300 (now published as UFC 3-340-01) is one of many sources this article used to create equations to approximate the pressures and impulses behind a protective barrier. It is a manual published by the U.S. Army that gives procedures for determining the blast effects from an explosion and the design of reinforced concrete structures. This manual gives plenty of data in the form of graphs and charts. Several graphs in the manual display curves for pressure or impulse versus distance from an explosive charge. The author used AUTODYNE3D to model and run simulations, using TM5-1300 for empirical data. The simulations were very robust in that they can do calculations for several charge weights, building heights, and distances from the charge to the barrier and from the barrier to the building. When working with simulations one of the most important aspects is the mesh size. Generally the smaller the mesh size the more accurate the calculations. However, with a smaller mesh size longer calculation times are needed. Two different mesh sizes are considered for accuracy; a 250-mm mesh and a 500-mm mesh. The computers and software used to run these

simulations were limited in processing power and were not able to calculate a mesh size smaller than 500 mm. However, when looking at the effect a blast has on a building a very sharp peak pressure does not affect the building as much as a large drawn-out peak pressure, making a larger impulse. Looking at both mesh sizes it can be calculated that there is a 37.5% error in the peak pressures due to an insufficiently small mesh size. Even given the calculated error, the results agreed with TM5-1300. In order to calculate the pressures and impulses behind the barrier Zhou used modification factors. A_P is the modification factor for peak pressure and A_I the modification factor for impulse. The following equations were used to calculate the modification factors.

$$A_P = P_{\text{with_barrier}}/P_{\text{no_barrier}} \quad \{2.1\}$$

$$A_I = I_{\text{with_barrier}}/I_{\text{no_barrier}} \quad \{2.2\}$$

$P_{\text{no_barrier}}$ and $I_{\text{no_barrier}}$ are the maximum pressure and maximum impulse, respectively, that occur on the building surface at ground level with no barrier between the charge and building.

With explosives, several values are needed to be able to scale a blast and relate similar blast effects. One of the more common values used is called scaled distance. The scaled distance creates a relationship between the distance from the charge and the charge weight. The following is a well-known equation for calculating the scaled distance, Z (Tinsley et. al., 2007).

$$Z = D/W^{1/3} \quad \{2.3\}$$

D is the distance between the explosive and the building and W is the charge weight.

Scaled distance can be plotted against pressure in order to see the effect of different

charge sizes. However, the geometry and composition of the charge, as well as the atmosphere, must be consistent. The following equations were used to calculate the modification factors for maximum pressures and maximum impulses.

$$A_{P_{\max}} = -0.1359 + (0.3272 + 0.1995 \lg(H_1/D)) \lg Z - 0.5626 \lg(H_1/D) + 0.4666 L_1/D \quad \{2.4\}$$

$$A_{I_{\max}} = -0.0274 + (0.4146 + 0.2393 \lg(H_1/D)) \lg Z - 0.5044 \lg(H_1/D) + 0.2538 L_1/D \quad \{2.5\}$$

where H_1 is the blast wall height, D is the distance between explosive and building and L_1 is the distance between the explosive and the barrier. Once the modification factors are calculated and combined with the values from TM5-1300, they can be inserted into Equations 2.1 and 2.2 above to calculate the pressure and impulse behind the barrier. The following equations are for the time of arrival, T_a .

For $H \geq H_e$,

$$\lg(T_a/W^{1/3}) = -0.0921 + 1.4806 \lg Z + 0.1388 \lg(H_1/D) - 0.0551 \lg(L_1/D) + 0.008 H \quad \{2.6\}$$

For $H < H_e$,

$$\lg(T_a/W^{1/3}) = -0.0921 + 1.4806 \lg Z + 0.1388 \lg(H_1/D) - 0.0551 \lg(L_1/D) + 0.008 H_e \quad \{2.7\}$$

where H is a point picked by the user on the side of the building and H_e is the vertical distance on the building shown in Figure 2.5.

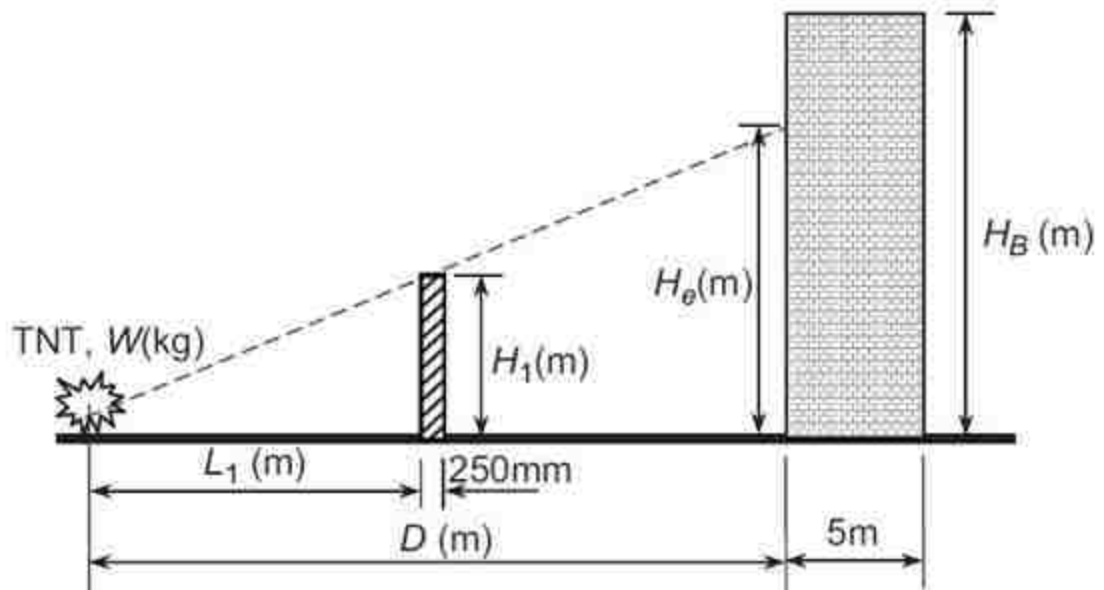


Figure 2.5 Blast layout configuration (Zhou et. al., 2007)

The following equation is for positive phase duration, T_o .

$$\lg (T_o/W^{1/3}) = 0.1699 + 0.9274 \lg Z + 0.1154 \lg (H_1/D) - 0.0793 \lg (L_1/D) - 0.0022 H \quad \{2.8\}$$

This research found that the effectiveness of a barrier is based on several factors: barrier height, distances between the explosive and the barrier, the distance between the barrier and building, and the height of the building. This research also made known that a barrier is effective at reducing the peak pressure from an explosive and delays the time in which the pressure wave arrives.

2.4 DUCTAL[®] – AN ULTRA-HIGH PERFORMANCE MATERIAL FOR RESISTANCE TO BLASTS AND IMPACTS (CAVILL ET. AL., 2006)

Lafarge, a leading research facility in building materials, has developed a new ultra-high strength concrete called Ductal[®]. This product makes use of a material called

reactive powder concrete (RPC). RPC is made up of the following materials; cement, sand, silica fume, silica flour, super-plasticizer, water and high-strength steel fibers. Ductal[®] concrete has a compressive strength of 160-200 MPa and a flexural strength of 30-40 MPa. Standard concrete compressive strength is usually 20-40 MPa and its flexural strength is usually 3-5 MPa. Ductal[®] is significantly stronger than standard concrete but there are downsides to Ductal[®]. The cost is significant and the process for creating the material is involved. However, the heat bath accelerates the strength gain reducing the cure time. Ductal[®] gets its strength from using less water in the mix, but with using less water comes a high risk that the object will crack. These cracks are called plastic shrinkage cracks and do not affect the structural integrity. To keep the object from these plastic shrinkage cracks, it needs to cure in a heated bath. A problem comes when the object is large. Lafarge deals with this problem by building several heated buildings. Sprayers are mounted in the tops of the buildings to keep the concrete wet and warm. Research showed that there is a fifteen-percent increase in strength when compared to non-heat treated concrete. Figure 2.6 shows the properties and typical stress-strain relationships for this material. According to Lafarge, to reach these material properties the concrete must be cured in a steam bath at ninety degrees Celsius for forty-eight hours.

Property	Standard	Heat Treated Ductal®
Fluidity	ASTM C230	Between 190 and 250mm after 20 drops:
Compressive strength	AS 1012.9	160 MPa
Flexural Tension: Modulus of Rupture	AS 1012.11	24 MPa
Flexural Tension: First cracking	AS 1012.11	20 MPa
Modulus of Elasticity	AS 1012.17	47 GPa
Shrinkage	AS 1012.13	< 500 μ strain after 56 days 0 after heat treatment
Density		2.450 kg/m ³

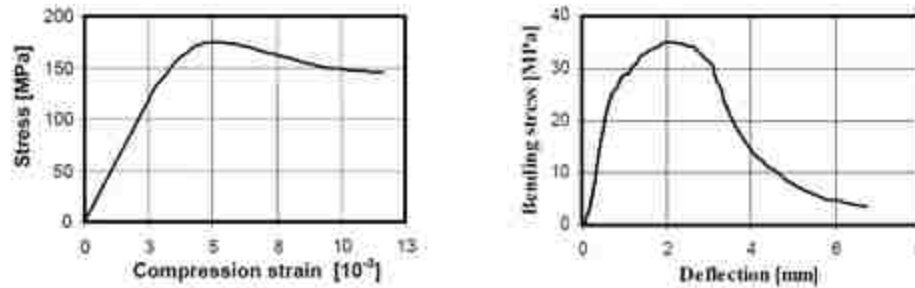


Figure 2.6 Typical force deformation response of Ductal® in compression and flexure (Cavill et.al., 2006)

In order to thoroughly test its product, Lafarge sent a team to Australia. The team led a joint effort between the VSL Australia Pty Ltd, a local construction company, and the Advanced Protective Technologies for Engineering Structures (APTES) group at the University of Melbourne. Several tests were done, including large-scale blast testing, fragment impact testing, close charge testing and ballistic testing. Cavill looked closer at the large scale blast testing and close charge testing. The large scale testing consisted of two separate blasts. These blasts used five tonnes of Hexolite each, which is equivalent to six tonnes of TNT. A total of seven panels were tested having the dimensions of 1 m wide, a span of 2 m and three different thicknesses of 50 mm, 75 mm and 100 mm. Five of these panels contained high-strength prestressing strands with a tensile strength of 1840 MPa. All other information about the details of the prestressing strands are

confidential. The configuration and results from the test of the seven panels can be seen in Table 2.1.

Table 2.1 Main observations, Woomera blast trial (Cavill et.al., 2006)

PANEL TYPE	Stand-off Distance	Recorded Deflection	Main observations
Stressed 100mm	30m	50mm in 37mm out 0mm	Virtually undamaged, no permanent deflection. Several vertical hairline cracks in front face of 0.1 to 0.2mm width, No fragmentation.
Stressed 100mm	40m	Laser No record 0mm	Basically undamaged, no permanent deflection, No fragmentation.
Stressed 75mm	40m	72mm in 55mm out 18mm in Laser	Intact, cracked with small permanent deflection, no fragmentation.
Stressed 50mm	50m	No record 0mm	Intact, shallow crack, no permanent deflection, no fragmentation.
Unreinforced 50mm	50m	>300mm	Fractured, no fragmentation
Stressed 75mm	30m	>300mm	Fractured, no fragmentation
Unreinforced 100mm	40m	280mm	Fractured, no fragmentation
Reinforced conventional concrete (40MPa) 100mm	40m	>300mm	Fractured, severe damage, fragmentation from back face

In another test done for close charge blasts, four panels were made and shipped to be tested in an unidentified English laboratory. Three of the four panels are manufactured by VSL Ductal[®] in Melbourne. These three panels were constructed with the same prestressed fibers used in the previous test. The fourth panel was a conventional reinforced panel. The conventional panel and one Ductal[®] panel were tested together with a close blast charge of 0.5 kg of Comp B. The remaining two Ductal[®] panels were tested using 3 kg of C-4. The results and test configuration can be seen in Table 2.2. Figure 2.7 shows the results of Panels 3 and 4 at the test done in England.

Table 2.2 Panel details for close charge tests (Cavill et.al., 2006)

Panel	Dimensions m	Material	Reinforcement	Explosive	Stand-off
1	1.0 x 1.0 x 0.1	Ductal [®]	High strength steel strands	3kg C-4	1.0m
2	1.0 x 1.0 x 0.15	Ductal [®]	High strength steel strands	5kg C-4	0.5m
3	1.3 x 1.0 x 0.1	Ductal [®]	High strength steel strands	0.5kg Comp B	0.1m
4	1.3 x 1.0 x 0.1	Concrete 50MPa	N20 at 75mm back face N20 at 150mm front face	0.5kg Comp B	0.1m



Panel 3 (Ductal[®]) front surface after explosion
No cracks



Panel 4 (conventional reinforced concrete) front surface after explosion - Slight cracks



Panel 3 rear surface after explosion
- Very slight scabbing at the surface of the panel.
- Minor cracks through the panel.
- Structurally undamaged.



Panel 4 rear surface after explosion
- Heavy scabbing, reinforcing bars exposed.
- Cavity approximately 480 mm x 300 mm, with a maximum depth of 50 mm (1/2 section depth).

Figure 2.7 Test panels 3 and 4 after close charge explosion (Cavill et.al., 2006)

The product has shown that it is very good at creating little to no secondary debris in a close blast situation and stands up well to large blast testing. When looking at the two

tests a strong case can be made that Ductal[®] is a very good candidate for building better blast-resistant construction.

2.5 ENERGY TRAPPING AND SHOCK DISINTEGRATION IN A COMPOSITE GRANULAR MEDIUM (DARAIO ET.AL., 2006)

This research looked into new composite materials and their ability to mitigate blast energy. In other research done by Daraio, iron shot collected as waste from a metallurgical plant was used in the design of explosive chambers and tested against explosive blasts. These tests had good success at mitigate blast energy and can reduce the amplitude of the shock when tested against a contact charge. Granular materials, such as those discussed in “Shock Mitigation by ‘Soft’ Condensed Matter” (Nesterenko, 2003), produce a nonlinear behavior. This nonlinear behavior influences the shock wave and wave propagation through a medium. This was the first report of impulse energy confinement done experimentally. It was found that energy was being trapped within the “softer” portions of the composite chain and was slowly released in the form of weaker separated peak pressures over a longer period of time. See Figure 2.8. The first three lines are sensors placed in the ensemble of beads to measure pressure. The bottom line is the pressure that reaches the wall. In the upper right-hand corner is the amount of pre-compressive force on the beads. On the y-axis the scale is 1 N per division.

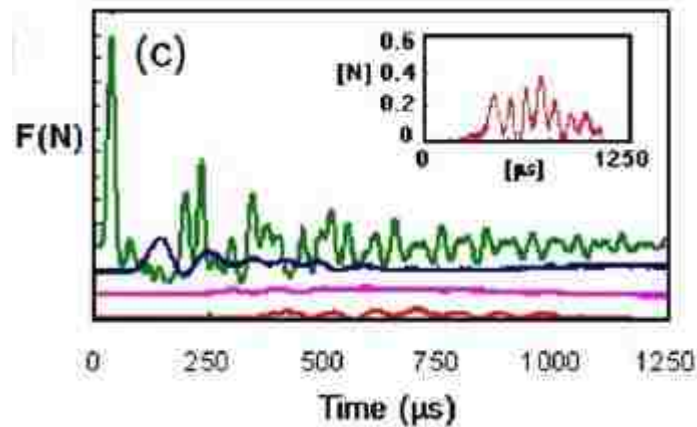


Figure 2.8 Pulse trapping in the composite granular protector with two PTFE sections (Daraio et.al., 2006)

A three-dimensional, nonlinear composite structure could lead to ultra-short pulse propagation from a shock wave. Taking the first step, this research studied the one-dimensional case for a fundamental understanding of the complex media. So how is this composite structure formed? For this experiment, the author used thirty-two spherical beads to create a “granular container” for pulse trapping. Twenty-two of these beads were of a high-modulus large mass stainless steel. The other ten beads were of a low-modulus small mass polytetrafluoroethylene (PTFE). The bead diameters were a uniform 4.76 mm, and different configurations had been investigated. Four piezo-sensors were used in the system of particles, allowing the time-of-flight calculations of the pulse speed. Two striking rods were used to create the waves moving through the system. To create a single solitary wave a 0.47-g Al₂O₃ rod was used and for shock-type loading a 63-g Al₂O₃ rod was used. It should be noted that when a solitary wave passes through a system going from a region of higher elastic modulus or higher mass to a region of lower elastic modulus the impulse decomposes into a train of solitary pulses. In other words, no

reflected wave is propagated back. However, if the solitary pulse goes from a region of low elastic modulus to a region of high elastic modulus it divides into two and no impulse disintegration beyond is observed. The testing done by this group proved mathematically and verified experimentally that blast energy can be trapped and slowly released, but the ability to do this depends largely on the particle arrangements. It was also proven that if the material is magnetically pre-compressed the signal is divided into several subdivided pulses, reducing the impulse even more. The authors came to this conclusion based on numerical simulations and attributed this effect to the high gradient of particle velocity near the interface.

2.6 SHOCK (BLAST) MITIGATION BY “SOFT” CONDENSED MATTER (NESTERENKO, 2003)

This research by Vitali F. Nesterenko looked at applications of “soft” condensed matter for blast mitigation. Nesterenko looked for relatively cheap, easily-available manufacturing process by-products that are highly nonlinear and heterogeneous to mitigate blast pressure. It is important to know how a structure will respond to impulse loading caused by a blast wave in order to prevent damage to the structure. When a structure encounters impulse loading, the response of the structure can be represented by an oscillatory system. Three responses can occur, represented in Figure 2.8; the response that occurs depends on the natural period of oscillation of the structure. The first response, (a) in Figure 2.8, is a short triangular pulse of shock pressure. It determines the maximum displacement and maximum stresses in the structure. For this specific case the application of “soft” condensed matter to tailor the impulse has no effect. The second

response, (b) in Figure 2.9, is a step function. In this case, maximum amplitude is determined by a pressure maximum and is equal to two static displacements. For this case, the more the amplitude of pressure is reduced, the better the blast mitigation will be. The final response, (c) in Figure 2.8, is a ramp function, which has a tendency to decrease with the increase of the ratio τ/T , where τ is time and T is the natural period of oscillation.

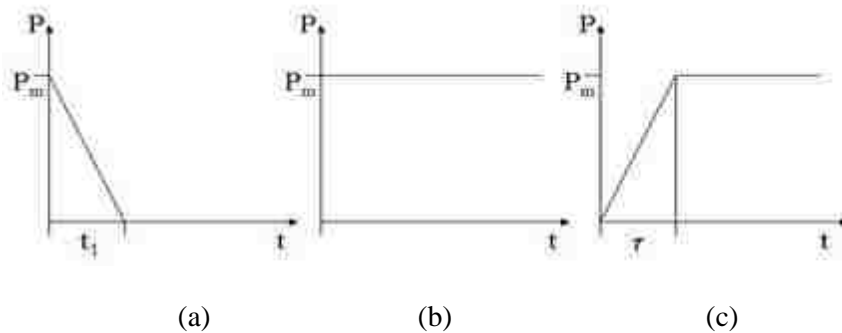


Figure 2.9. Three types of impulse loading $P(t)$: (a) triangular pulse with sharp front and duration $t_1 \ll T$, (b) step function with sharp increase of pressure and (c) ramp function with finite time τ of pressure increase. $P(t)$ represents pressure in a reflected shock wave(Nesterenko, 2003).

Nesterenko concluded that tailoring the pressure pulse with “soft” matter should be useful for mitigation of blast effects if it is possible to make the duration of impulse longer than the natural period. Therefore, it is very difficult to use this blast mitigation technique on large buildings because it is not possible to make the duration of impulse longer than the natural period of vibration. What is possible is to take a smaller structure, which would decrease the natural period of vibration and place it at some standoff

distance away from the structure that needs to be protected and have these principles applied.

The testing done by Nesterenko made use of two identical steel boxes. Both boxes had 0.5 kg of explosive (RDX) placed inside the box. In box “a” the explosive charge was placed in the center of the box and the box was closed. In box “b” the charge was again placed at the center of the box but sawdust of density 100 kg/m^3 was placed around the charge. One at a time, the charge within each box was detonated. Figure 2.10 shows that the sawdust mitigated the pressure enough to keep the box from breaking apart. Several interesting facts were found by doing this testing. Thermal conductivity of the material had no effect on mitigating the blast. It also was determined that an air gap between the explosive charge and the medium had no effect on the mitigation. The main factors that do contribute to the mitigation of a blast are the density, porosity and relative geometrical size of the medium. When trying to mitigate the pressure wave, it is important to note that there is a critical thickness for the damping medium. The porous barrier thickness must exceed six to eight diameters of the explosive charge. Nesterenko’s equation to calculate the critical thickness of the damping medium, H^* , in mm is

$$H^* = 216P_m^{0.6}t. \quad \{2.9\}$$

where P_m is maximum pressure, in MPa, and t is time, in ms.



Figure 2.10 (a) Catastrophic failure of steel structure after inside explosion in air and (b) confined explosion in the same structure filled with sawdust. Explosive (RDX) mass was 0.5 kg in both cases, wall thickness of containers 3 mm, side 0.7 m, sawdust density 100 kg/m³ (Nesterenko, 2003).

Nesterenko made it known that using something as cheap and readily available as sawdust can significantly reduce the blast wave propagation. However, can it be even better? Nesterenko has written several papers on organizing the porous state. He found that using multi-porous materials can change a step-function loading to ramped loading by acting on the maximum pressure, thus reducing the maximum stress two times and preventing spalling. A multi-porous material is a combination of large and small particles that have different moduli of elasticity. A multi-porous material or two different porous materials mixed together works very well to absorb energy. Nesterenko looked at hollow spheres or cylinders, made from low-strength materials like plastic or paper shells, to be mixed in with a much stronger material like iron shot. When the shock wave passes through the media the plastic crushes much easier, starting the energy absorption, and then the compressed steel shot absorbs a large amount of the remaining energy as it is compacted. Not all porous matter will automatically ensure effective shock absorption. It

is possible that an application of low-density porous layers can increase the shock pressure in a barrier, thus rendering more damage.

2.7 SCIENTIFIC PRINCIPLES (BREWER, 1999)

This online article gives a basic understanding of concrete. Concrete is a complex mixture of several materials one of which is cement. Cement is made by burning limestone and clay together at high temperatures ranging from 1400 to 1600 degrees Celsius. This powdery mixture is then combined with water to form a binder. This binder is mixed with a filler such as aggregate to form concrete. Approximately 70% to 80% of a concrete mix is made up of aggregate. The aggregate is ground before being added to the mix. By varying the granularity the mix density will change, contributing to the strength of the concrete. The more fine the aggregate powder the higher the density and the strength of the concrete. Adding water to the mix starts a process called hydration. Hydration is a chemical process where cement forms chemical bonds with water molecules to become hydrates. The amount of water in a mix plays a larger part in determining the strength of the cured concrete. A low water-to-cement ratio results in a high-strength mix. Admixtures, such as superplasticizers, are used to effectively mix the concrete when less water put into the mix. These admixtures can also be used to increase the life of the concrete, increase or reduce cure time, or change the color.

3 BLAST BARRIER DESIGN

The following sections discuss the design process for the concrete wall and media selection. They also demonstrate how the wall is constructed and how the media are added. The design of the wall is a particularly difficult problem to solve. The first problem to overcome is to decide what type of concrete is best suited for the project's needs. Next, what kind of shape should the barrier take? The shape of the barrier will have a large effect on the blast wave and will have a large effect on time and the cost of building the barrier. After a shape is selected, how will a hollowed cavity be placed into the center of the barrier, allowing a medium to be placed into it? The cavity was placed in the center of the barrier so it has sufficient strength to withstand a vehicle impact. Once the barrier is built, what is the best blast mitigating material to be tested in the barrier? When looking at wall designs several aspects are considered. First, it needs to be able to stop a vehicle that could be carrying a bomb. Second, it needs to mitigate the blast energy that occurs after an impact, enough to protect structures and people from high overpressure, and not create secondary debris. Third, it needs to have a hollow cavity in the center of the barrier for the blast mitigating material to be placed. Last, but not least, it needs to be easily distributable and cost effective.

3.1 CONCRETE

When considering the design and construction of the barrier, several different types of concrete, from a generic mix to a newer ultra-high strength concrete, come into consideration. Concrete is a standard product that is easily available. It is easy to manufacture and manipulate into different shapes and sizes. The author initially desired

to use an ultra-high strength concrete to hold the media, to reduce secondary debris and possibly help mitigate blast energy. Previously mentioned, Ductal[®] showed greatly desired properties when dealing with blasts. However, the expense of the product and the difficult curing process involved made Ductal[®] the wrong choice for this research. The author wanted to use a concrete that is easier to obtain and far less expensive. For these reasons, a standard inexpensive 41369-kPa-concrete formula is used for the construction of the barriers. See Appendix A for this formula. It should be noted that the formula sheet given in Appendix A is used as a baseline and the values are adjusted for each mix depending on the amount of concrete needed for the pour. For the development of the formula and all things concerning the concrete mixing, pour, construction and compression testing, the author used the expertise of three individuals: Ish Keener, Benjamin Gliha and John Bullock.

The first step in producing the desired concrete for this research is ordering one cubic yard, minimum order size, of concrete from Rolla Ready Mix. The concrete is mixed in the delivery truck with less water than necessary. When the truck arrives on site the appropriate amounts of water, super-plasticizer and, when necessary, long carbon fibers are mixed in. Once the concrete is mixed to the predesigned specifications, a slump test is done to determine the workability of the concrete. See Figure 3.1. A slump test fills a metal cone with concrete. The cone is quickly pulled straight up and the concrete is allowed to fall or "slump." Setting the metal cone next to the concrete allows the researcher to measure from the original height to the slump height and to obtain a percentage difference. If the concrete is 100% of the original height with the cone, or if

the height is less than 50% of the original height, then the concrete is considered unworkable (Brewer, 1999).



Figure 3.1 Slump test on concrete

In addition to a slump test, compression strength testing is performed to confirm the strength of the cured concrete. Figure 3.2 shows the results of the compression testing done for all three pours. The cylinders used for the compression tests did not have carbon fibers in them. For the first concrete mix, compression testing is done every seven days until a full cure is reached at twenty-eight days. There is no testing done for day twenty-one because there is little difference between day fourteen and day twenty-eight. These

data points are now used to plot strength vs. time, where a curve can be fit to anticipate how this design mix will cure. All mixes after the first are compression tested at twenty-eight days to ensure that a similar maximum strength is obtained from mix to mix.

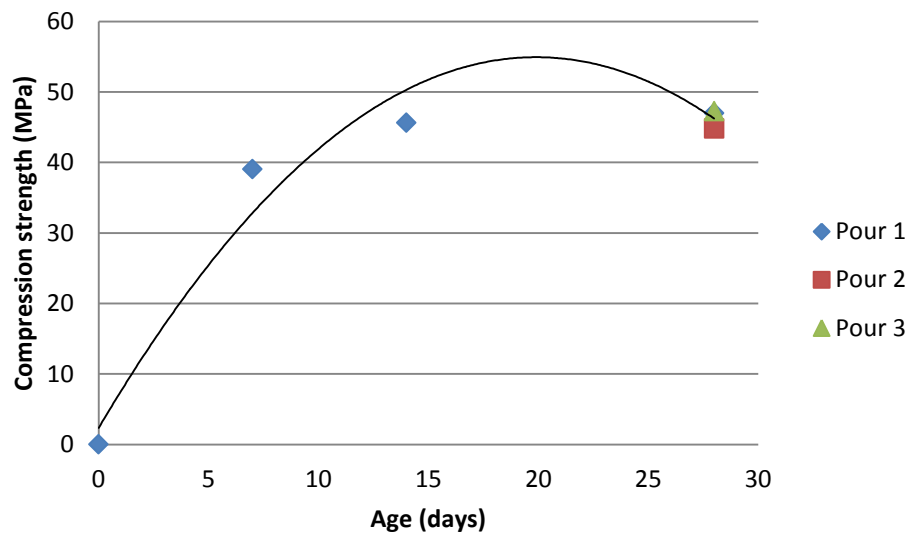


Figure 3.2 Compression strength testing plot

3.2 LONG CARBON FIBER (LCF) REINFORCEMENT

One of the abilities that the barrier design needs to have is the ability to prevent a vehicle carrying a bomb from breaching. In order to do this the concrete needs to be strong not only in compression but also in tension. In most cases, rebar is added to concrete to increase the tension capabilities. Many weaves or designs can be made with rebar that will add tensile strength in different directions. It is expensive and heavy to add significant amounts of rebar to concrete. In order for this research to save in weight, time

and especially cost, a product known as long carbon fiber (LCF) was used in place of rebar or steel fibers. In previous mixes done by Missouri S&T, research on LCFs showed that the fibers had a tendency to clump together in the mix and create voids, thus weakening areas in the concrete.

Three different pours are needed to make six barriers. Pour 1 makes only one solid concrete barrier without carbon fibers added to the mix. Pour two makes two barriers only one of which has LCFs added to it as shown in Figure 3.3. For this reason, the fibers did not get added directly to the concrete in the delivery truck. The concrete is poured from the mixer into nineteen-liter buckets, then poured into the framework. This method of mixing is slower and more physically intensive.

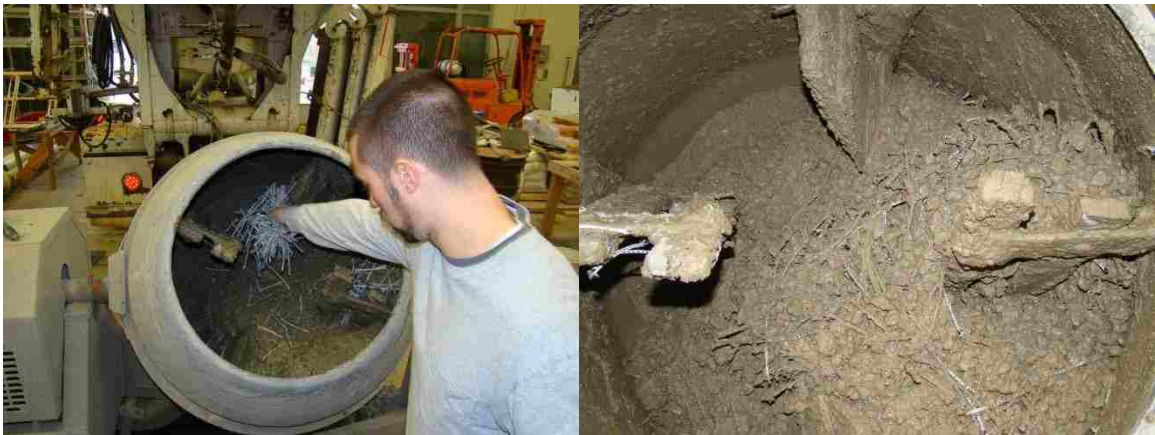


Figure 3.3 Mixing the LCFs by hand

Pour 3 makes three barriers. All have the concrete/fiber mix. For this pour the LCFs are added directly to the concrete in the delivery truck. The concrete in the truck is mixed to the required specifications before the LCFs are added. The LCFs and the

concrete are mixed for approximately fifteen minutes before casting the first barrier. The LCF dispersion is observed while pouring to ensure that no clumping is in the mix.

Three compression cylinders for this pour are checked for clumping of the LCFs after compression testing is complete. Mixing the LCF in the truck is a very efficient and easy method to disperse the fibers throughout the concrete. Once the concrete is formed, a vibrator is used to ensure that there are no voids in the evening of the concrete. The unit is used sparingly, no longer than five seconds for these mixes, to prevent separation of the heavier materials in the concrete.

Using the LCFs not only gives the concrete better tensile strength at the core of the structure in a similar fashion to rebar, but it also gives that better tensile strength to every part of the structure that it touches. The LCFs can be manufactured from a polyacrylonitrile (PAN) base or they can have a pitch base made from petroleum pitch. If the LCFs are PAN-based they can be made with either a high modulus (HM) or a high tensile strength (HT). If the LCFs are pitch-based they can be made for a general purpose (GP) or a high performance (HP). Carbon fiber properties are shown in Table 3.1.

Table 3.1 Carbon Fiber Properties (Volz et.al., 2010)

Fiber Type	Equivalent Diameter (in. x 10⁻³)	Specific Gravity	Tensile Strength (ksi)	Elastic Modulus (ksi)	Ultimate Elongation (%)
PAN HM	0.30	1.6-1.7	360-440	55,100	0.5-0.7
PAN HT	0.35	1.6-1.7	500-550	33,400	1.0-1.5
Pitch GP	0.39-0.51	1.6-1.7	70-115	4,000-5,000	2.0-2.4
Pitch HP	0.35-0.70	1.8-2.15	220-450	22,000-70,000	0.5-1.1

The LCFs used for this research were the Pitch GP, 102-mm-long fibers consisting of a 48K carbon fiber tow supported by a ribbed synthetic fiber system. A tow is an untwisted bundle containing several thousand fibers. The number 48 represents how many thousands of filaments are in the tow. An example of these LCFs is shown in Figure 3.4. The physical properties of the LCFs are listed in Table 3.2.



Figure 3.4 Long carbon fibers (Properma, 2014)

Table 3.2 Fiber properties used in this research (Properma, 2014)

Length	4 in. (102 mm)
Aspect Ratio	32
Specific Gravity	1.7
Absorption	3
Tensile Strength	600 ksi (4,137 MPa)
Tensile Modulus	35 msi (242 GPa)
Alkali, Acid & Salt Resistance	High
Electrical Resistivity	0.00061 ohm-in. (0.00155 ohm-cm)
Denier	54,000

The LCFs give the structure an added measure of secondary debris control. In other words, the LCFs reduce the spalling of the structure, decreasing the debris that can be thrown after a blast occurs. Testing done by Jeff Volz PhD, SE, PE at the Leonard Wood Institute developed two coatings for LCFs. These new coatings prevented the LCFs from balling in the concrete and creating voids. As part of this research the LCF reinforced concrete was used to make panels for impact and blast testing. The Blast testing included seven two-meter-square panels. The panels were one-hundred-sixty-one-millimeters thick. Three panels had steel reinforcement, two had steel reinforcement with an epoxy coated Cytec fiber and two panels with steel reinforcement with a polypropylene fiber. These panels were tested against a charge with a net equivalent weight of seventy-five pounds of TNT. In terms of amount of material lost fiber panels outperformed non-fiber panels almost by a factor of 10 in terms of material lost from the panel according to (Volz et.al. 2010).

3.3 CONSTRUCTION

Concrete is very durable and strong in compression. It is the compressive strength of concrete that makes it a good candidate for protection against an explosive blast. A high compressive strength would be desirable to be able to withstand the impact of a vehicle and explosion immediately after. It would also make it more difficult for shrapnel to make it through the barrier. The weakness of concrete comes when it is placed into tension, which happens in a blast. Concrete is also weak when a shear stress is placed on it. When a very strong blast wave propagates through concrete and reaches the back side of the object it reflects and another wave called a rarefaction moves back through the concrete, putting it into tension. The act of removing the material from the back side of a barrier by placing it in tension is called spalling. Spalling removes material from the center of the barrier where the shock wave first makes contact on the back side of a barrier. This material flakes off at a high speed weakening the structural integrity. The blast wave strength needed to cause spalling depends on the material properties of the barrier. Besides the material properties, the shape of the barrier has a great deal to do with reflecting or absorbing the blast. It is impossible to place a barrier in front of a charge and not have most of the blast wave be reflected. The shock wave from an explosive charge is moving so fast that the majority of the shock wave is reflected off the barrier before the shock is transmitted into the barrier. However, the main purpose of this research is to determine if a medium can be placed inside a barrier and absorb more pressure than a common barrier. The design of the barrier was not optimized for blast wave reflection. Considering time and cost, it was deemed better to keep the design simple and use a rectangle shape for this research. The overall dimensions for the barrier were three feet

tall by three feet wide by one foot thick. By using this simple design this author was able to use pre-made formwork that is part of the available supplies in the concrete lab at Missouri S&T. These pre-made forms saved a considerable amount of money and time for the project.

3.4 DESIGN

In order to test the blast mitigating media, there needs to be a way to hold each medium in place and subject it to a blast wave. This project was initially under the F4E initiative of the ALERT (Awareness and Localization of Explosives-Related Threats) project governed by the DHS, and in conjunction with other schools. The DHS needed a better way (than the common commercial barrier that have no blast protection) to protect its structures all over the world. The DHS set the initial design parameters: easy deployment for forward operating bases, mitigation up to a 114-kg-TNT-equivalent car bomb, cellular infill material contained within the barrier to absorb and impede a shock wave and no secondary debris. The barrier design discussed in Section 3.3 fulfilled these requirements. However, there needed to be a way to access the center of the barrier, and allow the cavity to be filled and emptied. This problem posed a particularly difficult challenge. How can a hollow cavity be placed inside of a concrete barrier and still keep the integrity of the outer structure as one piece? The simplest solution to this problem was to place a sheet of Styrofoam in the center of the formwork, and then to dissolve the foam from the barrier once the barrier has cured, leaving a cavity in the barrier. To achieve the desired thickness, two panels of fifty-one-mm white insulating foam were glued together and cut to the necessary size and shape. The bottom of the foam sheet was

cut in the shape of a V. See Figure 3.5. The dimensions were traced onto the foam, then cut with a wood saw.

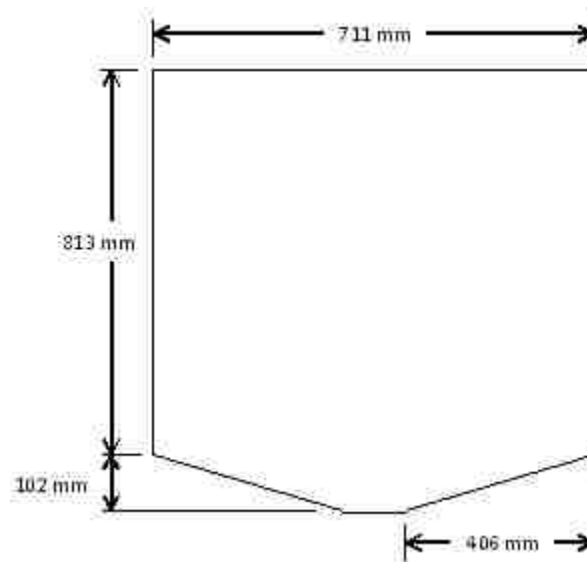


Figure 3.5 Foam cutout dimensions

Placing the Styrofoam in the formwork allowed the concrete to flow around the object and sit until the concrete cured. See Figures 3.6 and 3.7. This gives the bottom of the cavity a downward sloping plane along which a solvent could flow. The foam was held in place using flat metal wall ties that are placed through the foam, then secured in place by the formwork. In order to be able to remove the foam after the concrete had cured, a twenty-five-mm diameter by one-hundred-two-mm long PVC pipe was placed at the bottom of the foam. Two more PVC pipes of the same size were placed on top of the foam to allow the cavity to be filled. The two pipes on top of the foam were spaced

evenly to give access for a solvent to be poured into and sprayed into the cavity to remove the foam.

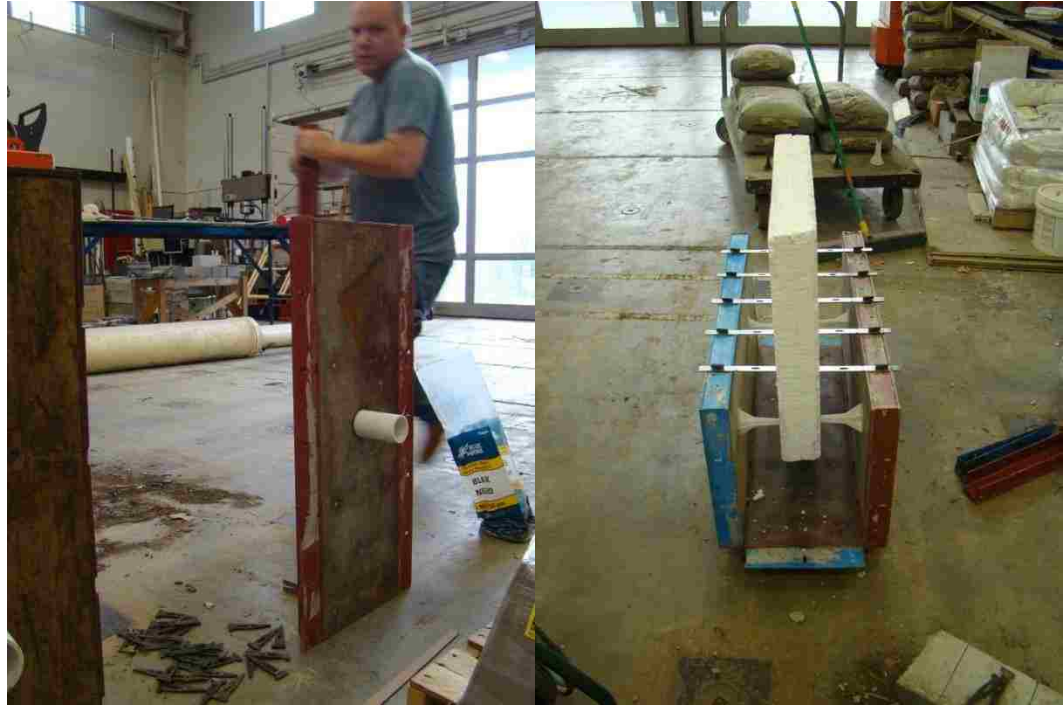


Figure 3.6 Construction of foam filler and framework



Figure 3.7 Frame and foam secured and ready for pour

Once the foam was removed, the barriers were allowed to vent overnight, allowing any remaining fumes and residue to escape. Once vented a small wooden plug was placed in the bottom pipe so the pipe can be filled with a fast-setting Quikrete® concrete of a similar strength to the rest of the barrier. The Quikrete® set hard in 20 minutes and was allowed to cure for 24 hours, allowing the concrete to reach 25% of its maximum strength. With the bottom pipe plugged, the medium was added to the barrier until full. Both pipes on top were filled with Quikrete® and allowed to cure overnight. It is noted that the PVC pipe in the concrete is a source of fracturing due to the inherent weakness at that point. There are also two rebar hooks placed in the top of the barriers to allow for lifting and moving the barriers. These, like the pipe, created an unavoidable inconsistency in the concrete. It is the authors belief that these negative effects will be minimal.

4. EXPLOSIVES PROPERTIES

When an explosion occurs, a large pressure difference is created. This pressure gradient is known as a shock wave and it moves through the air or objects at the speed of sound. As the shock wave moves away from the explosive, it does so spherically. If the charge is on the ground, it propagates through the air hemispherically. The greater the distance the shock wave travels from an event, the weaker it becomes. The best defense against a shock wave is to get as much distance from the blast as possible. The decay of the blast wave is exponential. When looking at the plot shown in Figure 4.1, the peak, P^+ , is known as the peak overpressure. The region above ambient pressure is known as the positive phase and the region below ambient is the negative phase.

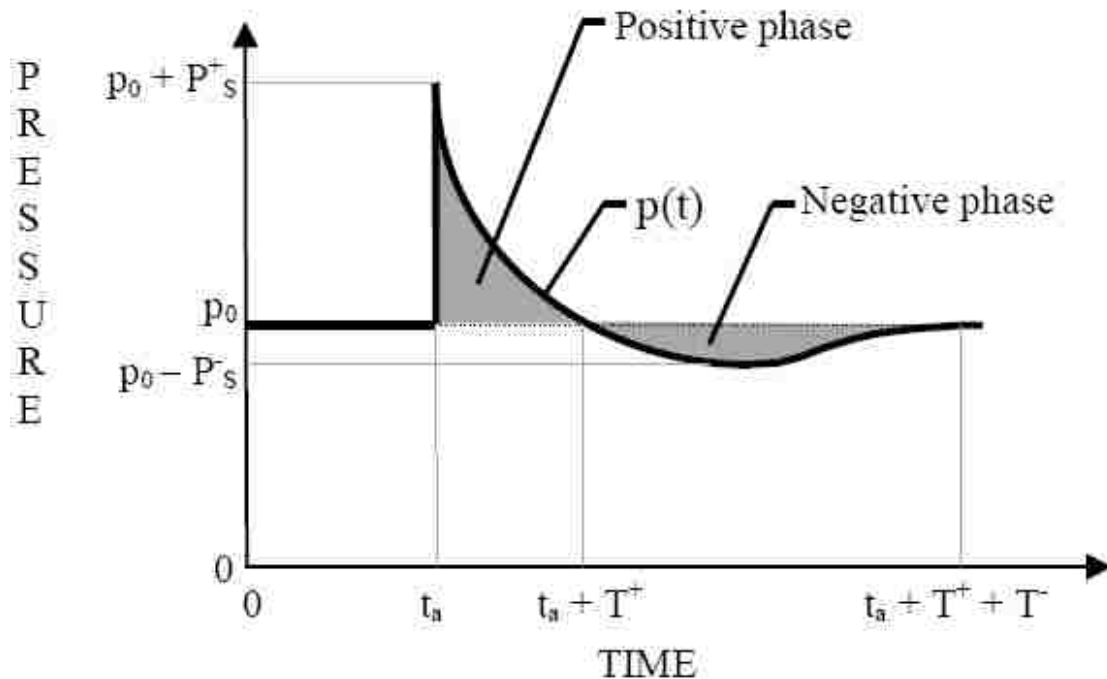


Figure 4.1 Pressure curve from a blast wave (Chaurasia, 2011)

This pressure curve can be represented by Equation 4.1.

$$p(t) = p_o + P_s + (1-(t/T^+))e^{-b(1/T^+)} \quad \{4.1\}$$

where p_o is the ambient atmospheric pressure, P_s^+ is the peak overpressure, t is measured from the time of arrival, and b is the decay coefficient. This research focuses on two aspects shown in Figure 4.1, the peak overpressure and the impulse. The impulse is the area under the curve for the positive phase of the graph. The impulse, like many properties of a blast, can be predicted but varies with the scaled distance. The scaled distance equation is frequently used to relate small-scale tests to full-scale tests. Because Missouri S&T does not have the space to permit full-scale testing for this research, Z is used to scale to an allowable blast size. Another important value when testing is N.E.W., the net explosive weight of TNT. Explosives have different specific energies; for this reason explosives can be compared against a standard, which is TNT. A computer code developed by the military called the Blast Effects Computer (BEC) is used to calculate several explosive properties. The peak overpressure, P , and impulse, I , can be calculated using the following from the BEC code (Swisdak, 2003).

$$\frac{P}{P_o} = \frac{808 \left[1 + \left(\frac{Z}{4.5} \right)^2 \right]}{\sqrt{1 + \left(\frac{Z}{0.048} \right)^2} \sqrt{1 + \left(\frac{Z}{0.32} \right)^2} \sqrt{1 + \left(\frac{Z}{1.35} \right)^2}} \quad \{4.2\}$$

$$\frac{I}{A} = \frac{0.067 \sqrt{1 + \left(\frac{Z}{0.23} \right)^4}}{Z^2 \sqrt[3]{1 + \left(\frac{Z}{1.55} \right)^3}} \quad \{4.3\}$$

where P_o is the ambient pressure, Z is the scaled distance, and A is the area.

It is important that the reader understands how a shock wave travels through a solid. When looking at a simple representation, a shock wave can encounter two conditions. The wave can pass from a lower-impedance-medium to a higher-impedance-

medium or the shock can pass from a higher-impedance-medium to a lower-impedance-medium. An example of the first case would have the shock traveling through the air and entering a concrete barrier. In this case, when the shock crosses the interface between the impedances there is a pressure increase and because the pressure increases, the velocity of the wave also increases. After the interface two shock waves continue; one travels through the higher-impedance-medium and one is reflected back through the lower-impedance-medium. Both of these shocks are of equal pressure. However, the pressure and velocity are higher than the original shock wave pressure and velocity. See Figure 4.2.

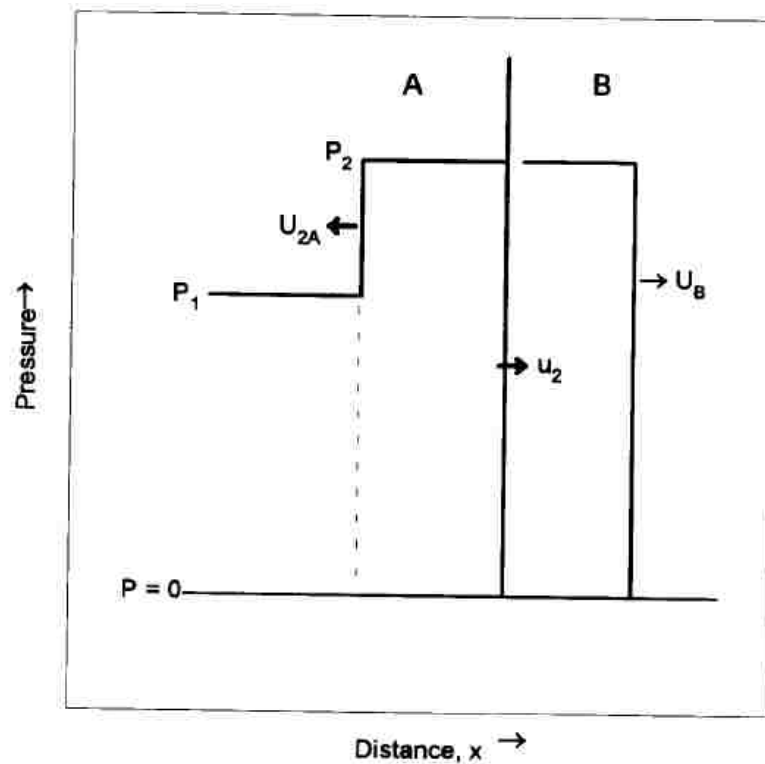


Figure 4.2 Pressure wave from low impedance to high impedance (Cooper, 1997)

In order to determine the properties on both sides of the shock wave the Hugoniot jump equation is used. The Hugoniot jump equation is formulated using the conservation of mass, energy and momentum equations. The equation for this specific case is.

$$P = \rho_0 C_0 (2u_1 - u) + \rho_0 S (2u_1 - u)^2 \quad \{4.4\}$$

where P is the pressure after the shock wave moves through the material, ρ_0 is the density, C_0 is the bulk sound speed, S is a dimensionless material property, u is the particle velocity before the shock and u_1 is the particle velocity after the shock.

For the second case the shock wave is going from a higher-impedance-medium to a lower-impedance-medium. After the shock wave reaches the interface of two materials, a shock wave continues through the lower-impedance-medium at a lower pressure and velocity than that of the original shock wave. Instead of a shock wave going back through the higher-impedance-medium, a wave called a rarefaction is created that travels back through the high-impedance-medium at a pressure and velocity equal to the shock wave going through the high-impedance-medium. See Figure 4.3.

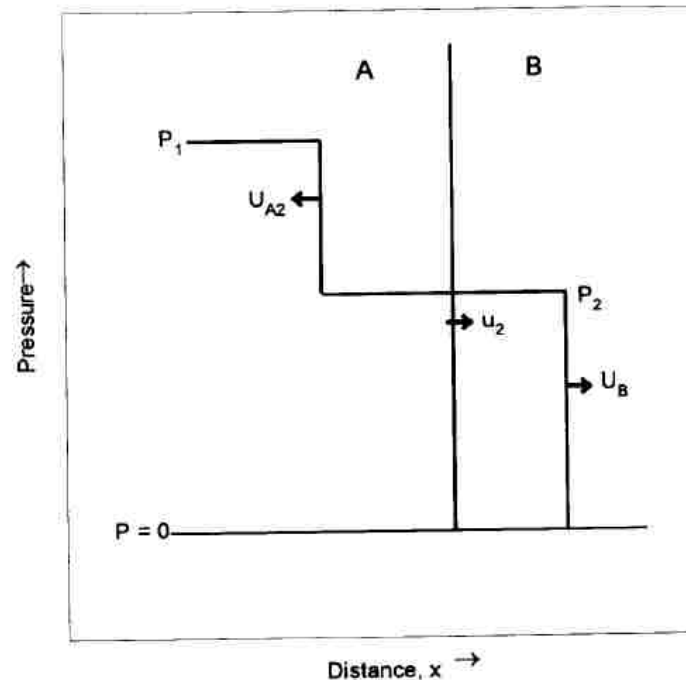


Figure 4.3 Pressure wave from high impedance to low impedance (Cooper, 1997)

A rarefaction is a shock wave that allows a shocked material to unload the pressure from the first shock wave and return the material to an ambient state. This pressure unload happens quickly and puts the medium in a state of tension instead of compression. This affect causes spalling. Understanding how a shock travels through different media impedances and using the Hugoniot jump equation, it is possible to track a shock wave through a barrier, estimate how long it will take to reach the back side and approximate the pressure.

4.1 BEC

Another important tool utilized by this research is the Blast Effects Computer (BEC) developed by the Department of Defense Explosives Safety Board (DDESB) (Swisdak, 2003). The BEC code bases most of the equations it uses on the scaled distance from Equation 4.2. These equations are generated by a curve that matches the empirical data. BEC Version 5.0 is used to calculate peak overpressure and impulse to obtain an idea of the levels that could be reached. Version 5.0 is capable of taking into account altitude, many different types of explosives, confinement, and ground or air blast. With these parameters set, the BEC gives values such as peak overpressure, impulse, time of arrival, reflected overpressure, reflected impulse, and positive phase duration. The author combined the equations from the BEC and from other sources into a single Matlab code. See Appendix B. Matlab is a fourth-generation numerical computing program developed by MathWorks (Matlab, 2012). Matlab has the ability to interface with other languages including C, C++, Java, Fortran and Python. These programs could also have been used to write the code in. However, Matlab is a very easy and quick language to code in. Besides numeric computation Matlab also has the ability to do data analysis and visualization and algorithm development. The Matlab code for this research uses several different equations to calculate the same value. These values along with the experimental data are compared and contrasted. All explosive equations have the inability to accurately present pressure at distances close to the explosive charge, because of the typical exponential nature of the equations used to describe blast pressure in air. It is also very difficult to take measurements really close to a blast without damaging the equipment; when the pressure wave expands from the explosive charge it takes a small amount of

distance for the pressure to become uniform. If the pressure is measured before this point, the readings are very chaotic. With the BEC code, as the scaled distance goes to $0.5 \text{ m/kg}^{1/3}$ or less the pressure goes to infinity. The equations can still be used at these distances. However, the smaller the scaled distance becomes the more error is introduced into the calculation. For the purposes of this paper, a scaled distance value below $1.7 \text{ m/kg}^{1/3}$ is not needed as this is the smallest scaled distance used for this research.

4.2 MEDIA SELECTION

There are an unlimited amount of materials and combination of materials that can be tested for blast resistant properties. When looking for different types of media for testing, the following material properties were considered in order to limit the selection size: density, porosity and relative geometrical size. These three main criteria are based on the author's literary research and are proven to mitigate energy from a blast (Nesterenko, 2003). The material hardness and geometrical shape of the media were also taken into consideration. The geometrical size was kept small to make it easier to add a medium to the barrier. The size of the medium will affect the density, which will affect the weight of the total structure, affecting the natural period. Another benefit of having a small particle size comes from the material's ability to absorb pressure while being compacted. Three different media were selected for this research: pumice, a porous rock that has sharp, hard edges; steel grit, a waste product of machine shops that has sharp, hard edges; foam, a thermal insulation that expands and hardens when exposed to air.

4.2.1 Pumice. Pumice is an igneous rock that it is formed by a volcano under intense heat and pressure. Like most volcanic rock, pumice is very porous and angular like broken glass. See Figure 4.4.



Figure 4.4 2-mm pumice

This porous sharp-edged rock could absorb a significant amount of pressure while being compacted by the shock wave. Then a rarefaction wave will travel back through the pumice, creating a dust cloud of spalled pumice powder. This powder then impacts the next surface with a severely reduced shock with a longer duration (Koontz, 1999). The pumice used in this research was ordered from Kramer Industries. As mentioned before, the size of the material was kept small for workability purposes, in this case 2 mm. The material has a bulk density of 449 kg/m^3 and is ordered in two twenty-three-kg boxes. It took about one and one-half boxes, or thirty-two kg, to fill the barrier.

4.2.2 Steel Grit. Steel grit was used for many of the same reasons as pumice.

See Figure 4.5.



Figure 4.5 2-mm steel grit

Unlike pumice, metals have a high tensile strength and will spall off in sheets. The idea is that since the steel grit particle size is small (2 mm), similar to the size of the pumice, and has sharp glass-like edges, a large amount of pressure will be reduced through spalling. The rarefaction will then turn the spalled steel into a cloud of metal and do less damage. This product was also ordered from Kramer Industries, with a bulk density of approximately 3925 kg/m^3 . The steel was ordered in 10 twenty-three-kg bags, all of which were needed to fill the barrier.

4.2.3 Foam. Several different foams were considered for testing. Research has shown that metallic flake foam covering a charge, with several times the charge diameter

thickness in foam, will mitigate blast energy. This author used a very different system to mitigate the blast pressure; the foam was sprayed inside a concrete barrier instead of covering the explosive charge.

This poses the next problem. What type of foam is best to use? Looking at many different types of foam and their application processes showed one consistent commonality; the cost. The foam and system needed to apply it ranged in cost from \$5000 to \$10,000. These foam systems were not within the budget; a cheap foam that could be easily obtained was needed for testing. Great Stuff™ (see Figure 4.6), an expandable insulating foam which can be obtained at any hardware store or Wal-Mart for approximately \$3 - \$4 per can, was the simplest and most cost-effective option.



Figure 4.6 Canister and foam sprayed on board to observe expansion

The cans come with an attachable straw that is designed to agitate the foam and make it expand. This straw was combined with a three-foot long tube in order to reach inside the barrier.

It took approximately 40 canisters at about 1/10 tenth the cost to fill a barrier with foam. Once the foam was sprayed into the barrier, the foam set overnight to cure. This way the foam was able to expand into every part of the barrier and harden.

5. TESTING METHODS

The main focus of this research is to determine if it is possible to use a “soft” material inside a barrier to mitigate blast energy. Section 5 discusses in detail the equipment and the methods used in testing. It is not the purpose of this research to develop an optimized system.

Missouri S&T has an inventory of instrumentation for the students to use in research and for instructional purposes. This includes things like SLR cameras, a Phantom high-speed video, a Cordin high-speed camera, oscilloscopes, PCB® pressure transducers, strain gages, accelerometers and seismographs. The most important data to obtain are the peak overpressure and impulse that occur behind the barrier. These data were acquired using two PCB® pressure transducers connected to a synergy Digital Acquisition System (DAS) computer. Pressure transducers need to be selected based upon what type of pressure needs to be recorded and what the maximum measurable pressure will be. Using the BEC computer, calculations were run to approximate the pressures that could be sensed by the pressure transducers so that transducers with the correct range and frequency responses could be chosen. See Table 5.1. Both PCB® transducers are set up to measure dynamic pressure, and have a part number 102B15. See Figure 5.1. These pressure transducers have a measuring range from 0 to 1379kPa psi.

Table 5.1 BEC approximation of expected test values.

SUMMARY TABLE

Explosion Site (ES)		Open Storage/STANDARD		Type of Weapon		Bulk/Light Cased: STANDARD	
Type of Explosive		Composition C-4		Total NEW (lbs)		1.50	
RANGE	TIME OF	INCIDENT	INCIDENT	POSITIVE	REFLECTED	REFLECTED	DYNAMIC
(meters)	ARRIVAL	PRESSURE	IMPULSE	DURATION	PRESSURE	IMPULSE	PRESSURE
	(ms)	(kPa)	(Pa-s)	(ms)	(kPa)	(Pa-s)	(kPa)
0.6	0.2	3272.5	167.5	0.4	24357.2	1600.0	7871.3
0.1	0.0	out of range	out of range	out of range	353504.2	23201.3	out of range
0.2	0.0	out of range	out of range	out of range	263208.1	15287.5	out of range
0.2	0.0	out of range	out of range	out of range	200045.4	11004.1	out of range
0.2	0.0	15052.9	300.6	0.2	157071.7	8401.9	57007.5
0.2	0.0	12652.4	250.0	0.2	126924.0	6689.7	44856.2
0.3	0.1	10853.2	217.6	0.2	104923.8	5495.5	36699.3
0.3	0.1	9440.7	196.2	0.2	88274.5	4624.6	30743.2
0.3	0.1	8042.6	179.1	0.2	72471.5	3827.4	25150.5
0.4	0.1	6930.8	168.7	0.2	60437.3	3241.8	20878.0
0.4	0.1	6025.7	162.8	0.2	51002.4	2796.7	17500.9
0.5	0.1	5276.5	160.0	0.3	43439.9	2448.9	14774.0
0.6	0.2	3272.5	167.5	0.4	24357.2	1600.0	7871.3
0.8	0.3	2162.2	192.2	0.8	14627.4	1165.5	4441.6
0.9	0.4	1498.7	227.7	1.4	9235.1	907.0	2630.2
1.1	0.5	1080.2	216.4	2.0	6080.9	737.6	1626.3
1.2	0.7	804.6	197.2	2.1	4155.6	619.0	1045.3
1.4	0.9	616.4	178.2	2.1	2936.2	531.8	695.6
1.5	1.1	484.0	161.4	2.0	2146.0	465.2	477.4
1.8	1.5	317.4	135.4	2.0	1223.0	370.7	243.5
2.1	2.0	222.9	117.1	2.0	767.2	307.3	135.7
2.4	2.5	165.4	101.9	2.3	520.4	261.9	81.3
2.7	3.1	128.4	92.6	2.6	375.4	227.9	51.7
3.0	3.8	102.7	84.8	2.8	284.4	201.6	34.5
3.8	5.5	65.9	70.0	3.3	165.5	156.2	14.9
4.6	7.3	47.1	59.5	3.6	111.5	127.3	7.6
5.3	9.3	36.1	51.7	3.8	82.3	107.3	4.5
6.1	11.3	29.0	45.7	4.0	64.6	92.7	2.9
6.9	13.3	24.2	40.9	4.1	52.8	81.6	2.0
7.6	15.3	20.7	37.1	4.3	44.6	72.9	1.4



← Cable attached here.

Figure 5.1 Pressure transducer 102B15

These transducers have a useful over-range of 2758 kPa, a maximum pressure of 6895 kPa, sensitivity of 3.6mV/kPa and a maximum flash temperature of 1650 degrees Celsius. The transducer uses a quartz crystal to translate the pressure it feels into an electrical signal that is sent to a DAS computer. See Appendix C for all properties of the transducer. Cables are run out the back of the transducers on the ground to the Synergy data acquisition system that records the data. See Figure 5.2.

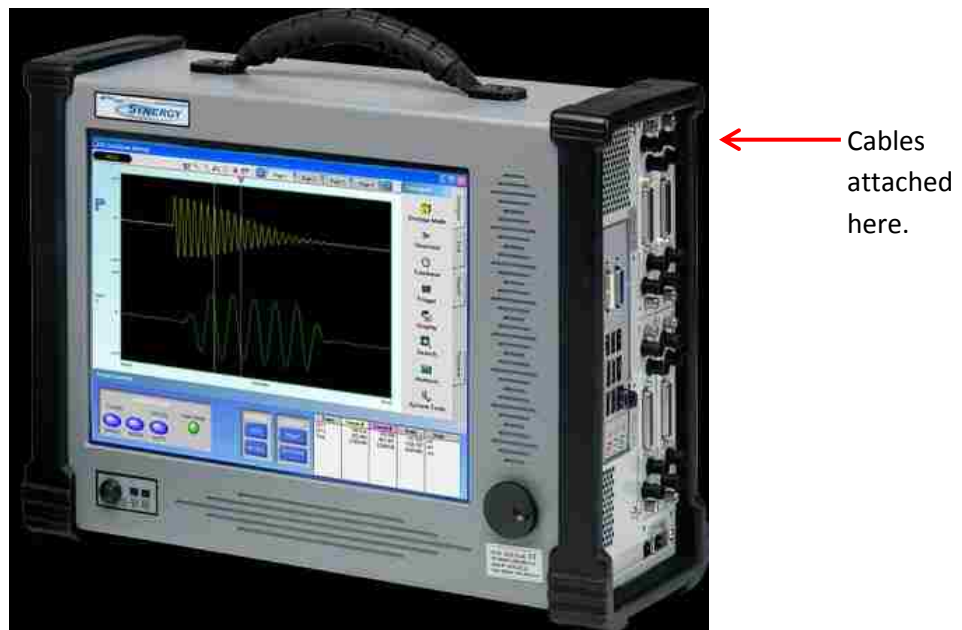


Figure 5.2 Synergy DAS computer

The Synergy version 5.0 data acquisition system houses four input modules which have 4 channels each, totaling 16 channels. Each of these channels has the ability to record 2 million samples per second. If all channels are recording, they can stream directly to the disk at 500,000 samples per second. The data acquisition system has the ability to make use of up to 64 channels that can record at 100,000 samples per second. It

is possible to use strain gages and accelerometers on the back of the barriers to capture any distortion or movement that could be transmitted through the barrier but, due to time and a possibility of destroying the devices, they were not used.

All testing was performed at the Missouri S&T Experimental Mine. There are several sites used for testing at the mine. This research made use of the aboveground and underground testing areas. The underground testing site is a small mine system that is used mainly to contain shrapnel or larger explosive charges. The underground site layout can be seen in Figure 5.3. It is more difficult to test underground because of the confinement and there is not enough natural light underground to be able to capture video of the event. If it is necessary to have video, special lighting and equipment are needed to add light and protect the camera. The camera needs to be protected from shrapnel and the blast wave that creates extreme pressures in the confined space.

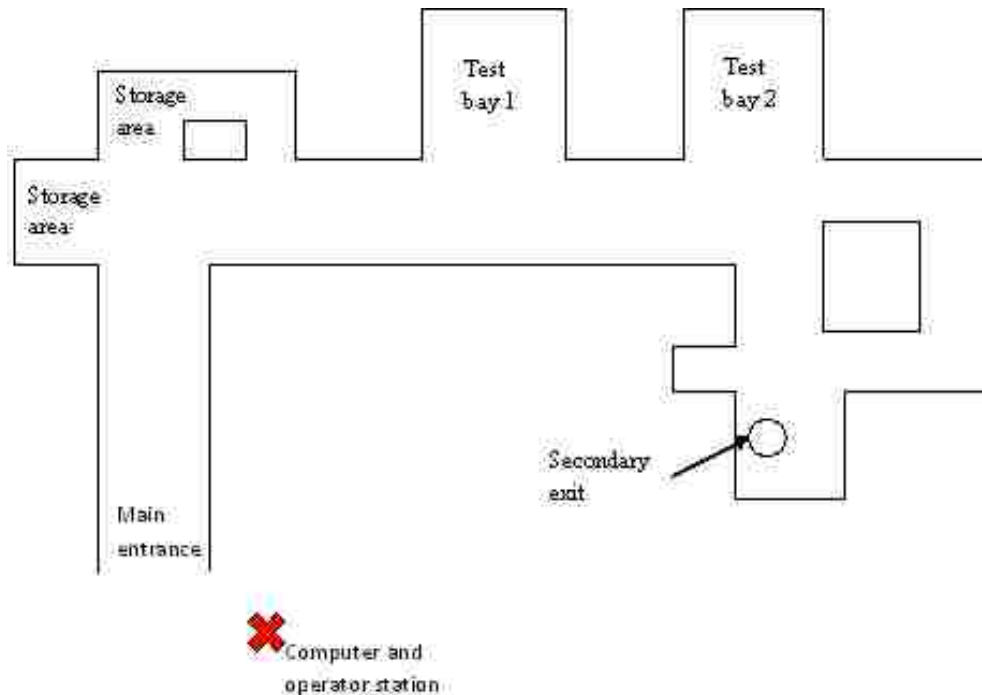


Figure 5.3 Underground test facility layout

Testing for this research started in the underground facility because of the climate-controlled atmosphere that it offers. In an effort to save time and money, the lights and video for the underground testing are not used. Once testing commenced it was noted that the pressures being measured were far above the predicted values from the BEC. This was assigned as due to the shock wave reverberating off the walls of the mine. The first obstacle to overcome was how to hold the barrier in place and not affect the test. The floor in the mine is not level and the blast wave pressure calculated was strong enough to move the barrier. Therefore, to keep the barrier from falling over a metal frame was constructed out of seventy-six-millimeter-by-seventy-six-millimeter steel angle. The frame was bolted to the floor using anchor bolts to keep it from moving, and then the barrier was set into the frame using a skid steer forklift. Once the barrier was in place the

data acquisition system was set up outside the mine in a place unaffected by the blast. See Figure 5.3. The cables were run from the data acquisition system along the wall of the mine to Test bay 1. The distance is less than thirty-one meters so the signal did not need to be boosted or modified in any way. The cables were attached to the pressure transducers which were placed in a stand made to hold them. For both aboveground and underground testing, the cables are sandbagged up to eighteen meters away from the charge to protect the cables and signal from the blast. Transducer 1 was placed in front of the barrier and Transducer 2 was placed behind the barrier, with the explosive charge positioned between the transducer and the barrier. This was done to measure the unaltered pressure and the pressure that is changed by the barrier. Three different standoff distances were tested: one and one-half meters, six hundred and nine millimeters and three hundred and five millimeters. Transducer 1 was moved to three different distances to keep the transducers equal distance from the charge. With the limited space, the transducer behind the barrier was kept at one and one-half meters from the face of the barrier to the front of the transducer. See Figure 5.4.

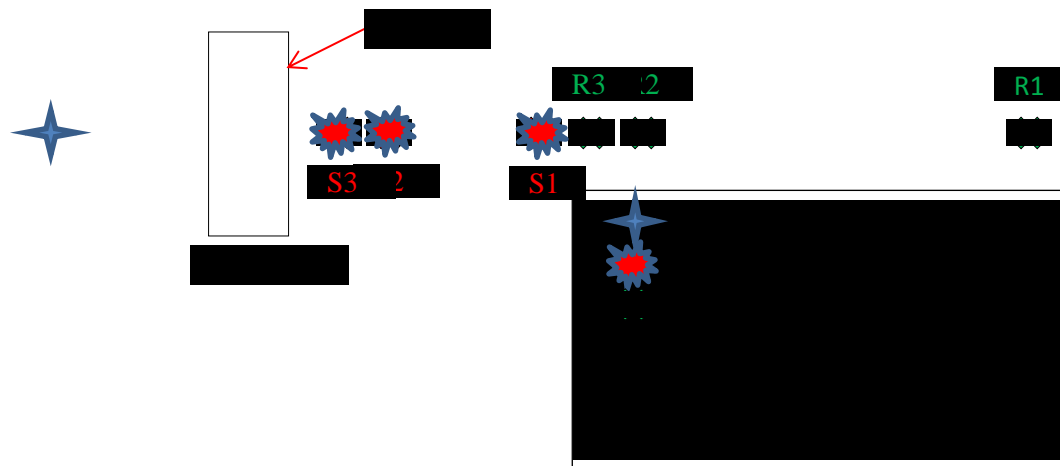


Figure 5.4 Experimental test layout

A wire was run along the ceiling to suspend the charge and make it easier to move the charge and center it with the face of the barrier. The first test had a standoff distance of five feet and a solid concrete barrier. See Appendix D to see a matrix of all test setups. After the transducers were set in place, the data acquisition system was calibrated to each specific transducer and tested to see if the data acquisition system is receiving a signal. See Appendix E to view the steps for calibrating the DAS data acquisition system. The charge, which was pre-made by the author to 680 grams, had a detonator pushed into the center of the charge and taped in place so it did not move. Then the charge was suspended in the correct position. With the charge in place, the test area was evacuated to a safe location. The lead shooter connected to the firing box, an audible warning was given and the data acquisition system recording started. The sample rate for this testing was one million samples per second, which limited the time the data acquisition system can record to one second. Because the data acquisition system continuously records, a trigger was used to stop the recording so the data was not overwritten. In order to capture

the whole event, 20% of the recorded samples was taken before the trigger and 80% is recorded after the trigger. The data was then saved in the data acquisition system and transferred to a flash drive when testing was finished for the day. Using a ventilation hood that rolls over the secondary exit, it takes approximately 20 minutes for the underground test site to clear of smoke. This vent hood was rolled off of the secondary exit before each test so it was not damaged. Once cleared the lead shooter gave the all clear before the rest of the team to set up for the next shot. Due to unforeseeable circumstance of the shock reverberation in the underground site, it was necessary to move the testing to the aboveground site. See Figure 5.5.

Testing at the aboveground site is similar to the underground site except the testers go inside of a blast bunker with all the equipment to run the test. The aboveground site requires much less cable since the cabling does not need to be run outside of the tunnel system. The site allows for a maximum charge size of 1kg. The site has a blast bunker where all the test equipment can be set up for recording. See Figure 5.5 for the aboveground site layout.

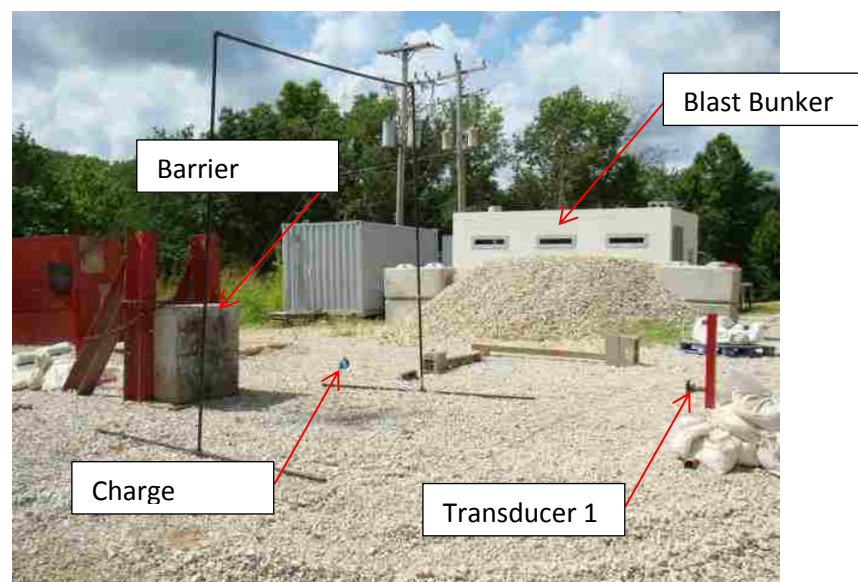


Figure 5.5 Aboveground test site

Because the testing moved above ground, additional equipment was used. Before testing commences on this site a skid steer loader is used to level the ground to minimize the interference to the signal being reflected. In order to obtain a better understanding of what is happening during the event, a Phantom camera was also used to capture the explosions in a high-speed digital format. The research utilized the Vision Research Phantom V10.1 high-speed digital camera with a CMOS sensor and a Tamron SP AF aspherical 28-75mm zoom lens. The camera is operated in accordance with the Phantom Camera Control Software Help Manual Revision 1. The step-by-step procedure can be found on Page 95 of the manual and can be used as a checklist for setting up the camera. Utilizing the procedures outlined in the manual, a black reference is done to obtain the highest quality images possible. The overall set up of the camera consists of placing it high enough on a tripod to see through the blast shelter window at approximately 14 meters from the charge. The resolution and frame rate were adjusted to obtain a wide-frame and detailed picture. This enabled the camera to capture both transducers, the charge and the barrier. It is more difficult to test with the camera because the trigger used for the data acquisition system could not be used to trigger the camera as well. This meant the camera had to be triggered manually. With the transducers set up, cables run, and the charge hung from a metal frame, the audible warning was given and the team moved inside the bunker. The shot-wire was connected to the firing box and a countdown was given by the person pressing the button to fire the shot. When the countdown (five down to zero) reached two, one of the pre-assigned team members activated the camera to capture the event. The charge was set off on a count of zero. The camera is set up much like the data acquisition system in that 20% of the recording time was captured

before the event and the other 80% is captured after the trigger. In between each shot, the video recorded was shortened to just the desired event and saved in a new file for download later. Testing aboveground is more time-efficient because there is no wait time for explosion gases to clear. Once the data has been acquired, the setup for the next shot begins. After every shot, the two-inch rock that makes the floor of the aboveground test site was smoothed out manually and the hole created filled in.

6. DATA ANALYSIS

This section makes use of the data acquired by the methods described in Section 5. In order to help keep track of the data, all peak overpressures and the times they occurred were recorded by the author. The temperature, relative humidity, barometric pressure, altitude, dew point and wind speed were recorded every day of testing. See Appendix F. Appendix D is a test matrix that shows all the tests done and the settings and surroundings for each test. Also included in the data is a column that tells if the barrier fell over. When testing underground the barrier was set in a frame that encompasses the outside edges on the back of the barrier. When the pressure wave from the charge pushes the barrier, the frame acts like a spring and propels the barrier forward. When looking at the aftermath of the test, the barrier would be face down on the ground and, in order to reset the test, the wires were moved to bring the skid steer forklift in to lift the barrier back into place. Several different methods were tried to prevent this from happening, with no success. This problem was solved when testing moves aboveground. A new system to support the barrier was used to great effect. The aboveground testing made use of two large I-beam supports that were secured in the ground. A large chain was used to hold the barrier against the I-beam supports. The barrier never fell over in an aboveground test.

Some problems arose when analyzing the data collected from the underground testing. Transducer 1 which is in front of the barrier, showed significantly lower pressures than Transducer 2 from behind the barrier. It is deduced from the layout of the mine that the pressure loss on Transducer 1 is from the pressure expanding down the hallway. This pressure difference for Transducer 1 changes significantly as the transducer

is moved closer, seven feet from the charge rather than ten feet. Moving Transducer 1 seven feet from the charge moves the transducer into the test bay and out of the hallway. It is also made clear that Transducer 2 experiences higher pressures from the shock waves reverberating at the back of the test bay. These pressures are much higher than the pre-calculated values from the BEC.

With a new data acquisition system and stable weather outside, the testing was moved to the aboveground testing site at the mine. Moving the testing aboveground eliminated the reverberation problem and the pressure difference seen underground. To address the problem of the barrier falling over, the author used a new method of supporting the barrier. No longer restrained by the underground dimensions, two large I-beam structures were placed behind the barrier and a chain was used to keep the barrier from falling forward. See Figure 6.1. Each of these barriers experienced a minimum of nine blasts each and the barriers' structural properties are affected from test to test. Every test done on a barrier places a large pressure gradient between the front and back side of the barrier. The barrier is supported on both edges forcing the barrier to flex most on the centerline. With every flex of the barrier micro-cracks are propagating through the concrete. When this happens enough, the cracks become visible and it is a good assumption that the barrier has been compromised. This affects Transducer 2 on the back side of the barrier. The more flex of the barrier, the larger the pressure reading. It is not possible to build barriers for every test conducted due to time and funding restrictions. For these reasons, and because the effects are considered to be small and insignificant until the propagation of surface cracks can be seen, it is deemed necessary that the barriers be reused.



Figure 6.1 Barrier chained to supporting I-beams

Testing aboveground was conducted according to Section 5. Each barrier was tested at three distances or until significant damage was seen on the barrier. It is for this reason Barriers 2 and 3, only have data at five feet. It is also noted during testing that a barrier with a medium incurs damages much faster than a barrier without a medium. See Tables 6.1 and 6.2 for Barrier configurations and notes on testing.

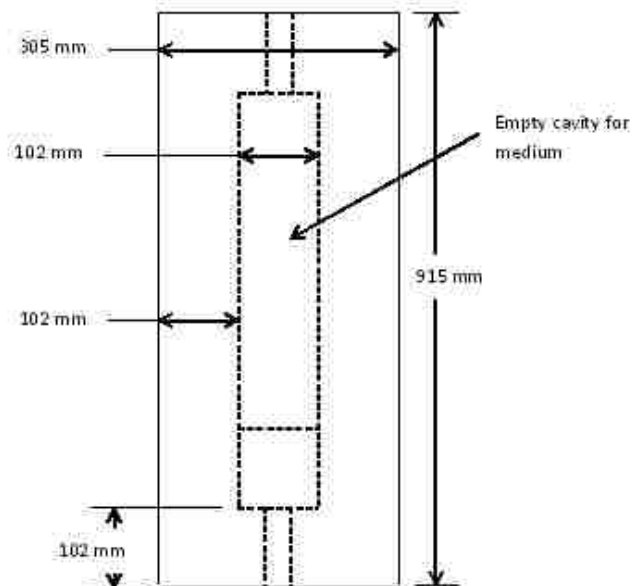
Table 6.1 Barrier configuration

Barrier	Medium	Carbon Fiber	Cavity	Weight of Concrete (kg)	Weight of Medium (kg)	Total Weight (kg)
1	NO	NO	NO	586	0	586
2	NO	NO	YES	468	0	468
3	NO	YES	YES	468	0	468
4	Foam	YES	YES	468	2	470
5	Pumice	YES	YES	468	23	491
6	Steel Grit	YES	YES	468	202	670

Table 6.2 Damage to barriers during testing

Barrier	Medium	Damage
1	NO	Small amount of damage caused by falling over underground. Never cracked or spalled. 9 tests below ground and 9 tests aboveground.
2	NO	Went 9 tests underground no cracking. Major cracking on 4th test aboveground.
3	NO	Went 9 tests underground no cracking. Major cracking on 3rd test aboveground.
4	Foam	No testing underground. Cracking started on 8th test. Finished all 9 tests.
5	Pumice	No testing underground. Cracking started on 9th test.
6	Steel Grit	No testing underground. Cracking started on 7th test. Finished all 9 tests

Barriers two through six were built identically with a centered cavity. Barrier one is solid concrete and was used as a control specimen. All barriers have the same outer dimensions. See Figure 6.2 and Figure 6.3 for a schematic. Three shots were recorded at each of the three distances from each barrier. The data at each distance were averaged and plotted on a graph.

**Figure 6.2 Side of barrier with cavity**

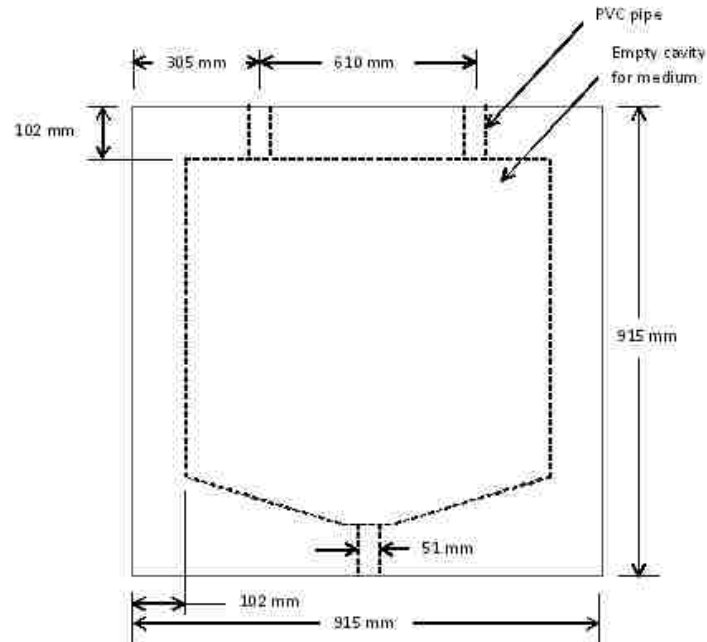


Figure 6.3 Front face of barrier with cavity

The pressures were taken directly from the DAS computer and placed in an Excel file, allowing the data to be further analyzed. The impulse was determined using the DAS computer by calculating the area under the pressure versus time curve. See Appendix G for a step-by-step process calculating the impulse. In order to calculate the impulse, the author picked two points on the curve and the data acquisition system calculates the area under the curve between the two points. The first point was placed in the same manner for every test, at the base of the first pressure peak where it is closest on the curve to zero. The second point was also placed at the same manner for every test, at the point where the curve first drops below the ambient pressure line and becomes negative. This happens after the peak overpressure. As the system is digital rather than analog, the pressure reported will not be exactly zero but very small, either negative or positive. The area is

calculated between the pressure curve and the imaginary line drawn by connecting the two points placed by the author.

Figure 6.4, Figure 6.5 and Figure 6.6 display the normalized impulses at distances 0.3 m, 0.6 m and 1.5 m, respectively. For every test two pressures were recorded. An unaltered pressure and the pressure affected by the barrier. To normalize the values graphed below, the pressure or impulse value that is affected by the barrier was divided by the unaffected pressure.

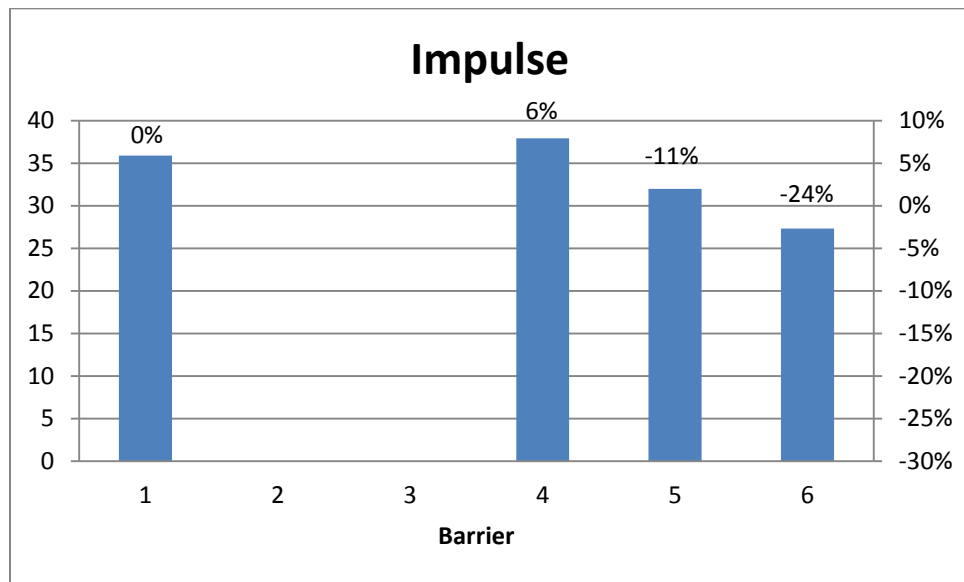


Figure 6.4 Normalized impulses at distance 0.3 m, showing percent impulse difference between the barrier and barrier 1

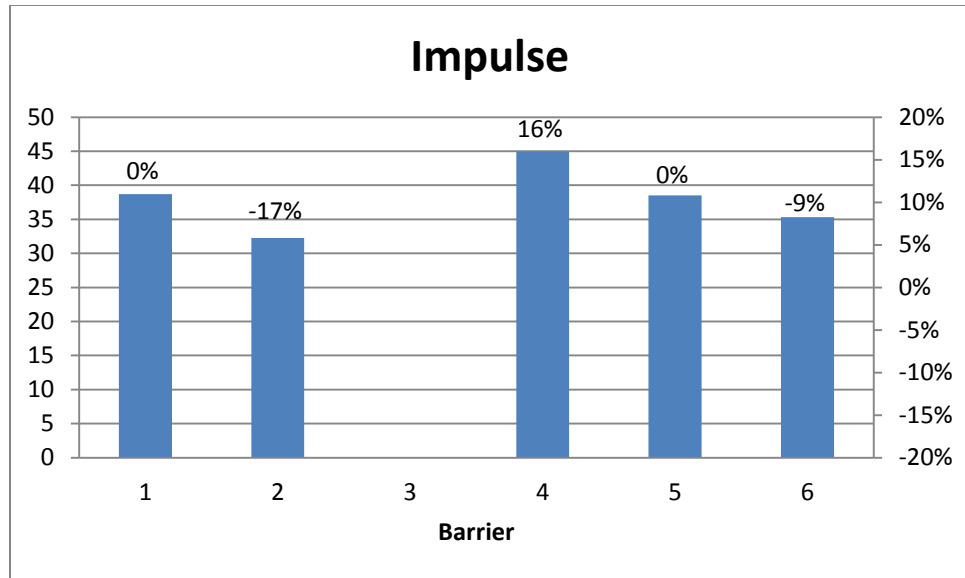


Figure 6.5 Normalized impulses at distance 0.6 m, showing percent impulse difference between the barrier and barrier 1

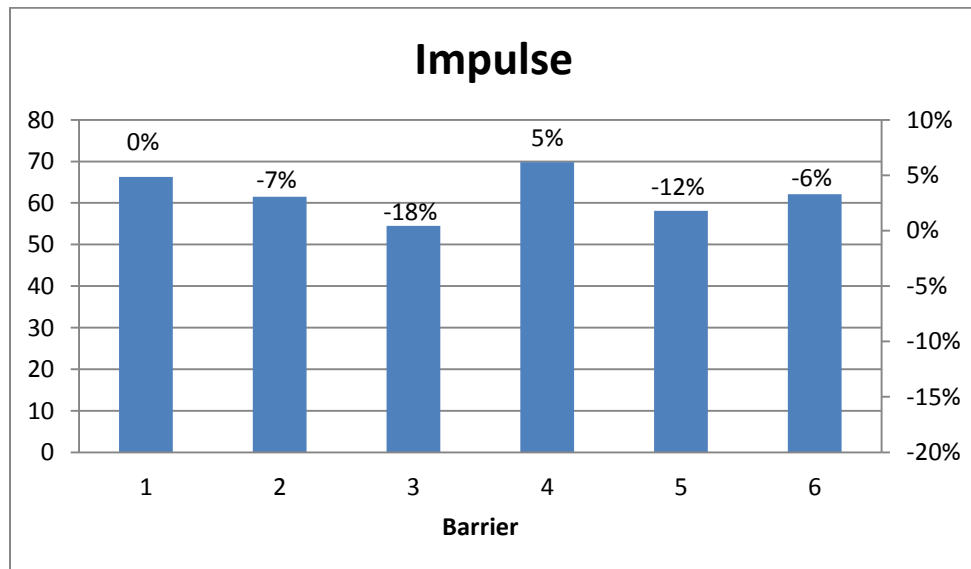


Figure 6.6 Normalized impulses at distance 1.5 m, showing percent impulse difference between the barrier and barrier 1

Figure 6.7, Figure 6.8 and Figure 6.9 display the normalized pressures at distances 0.3 m, 0.6 m and 1.5 m, respectively.

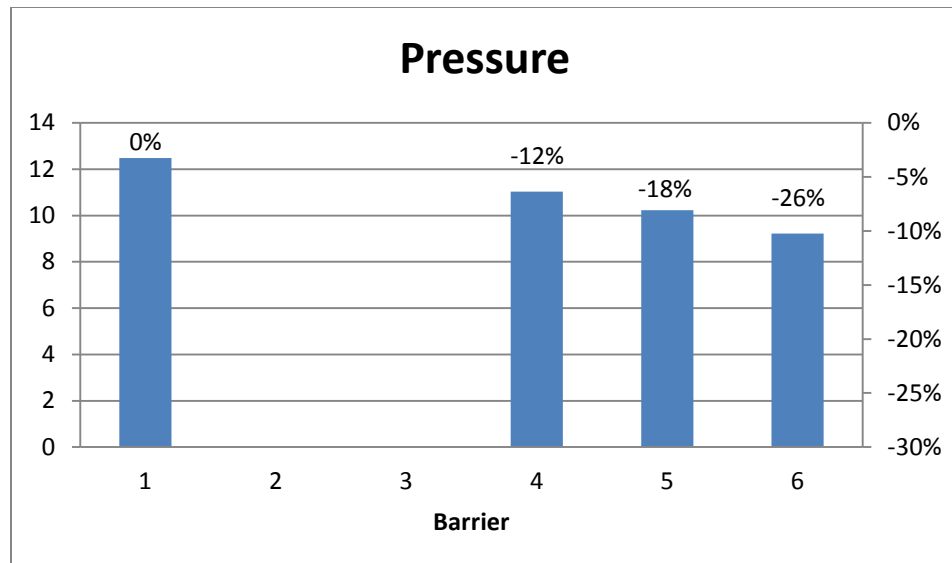


Figure 6.7 Normalized pressure at distance 0.3 m, showing percent pressure difference between the barrier and barrier 1

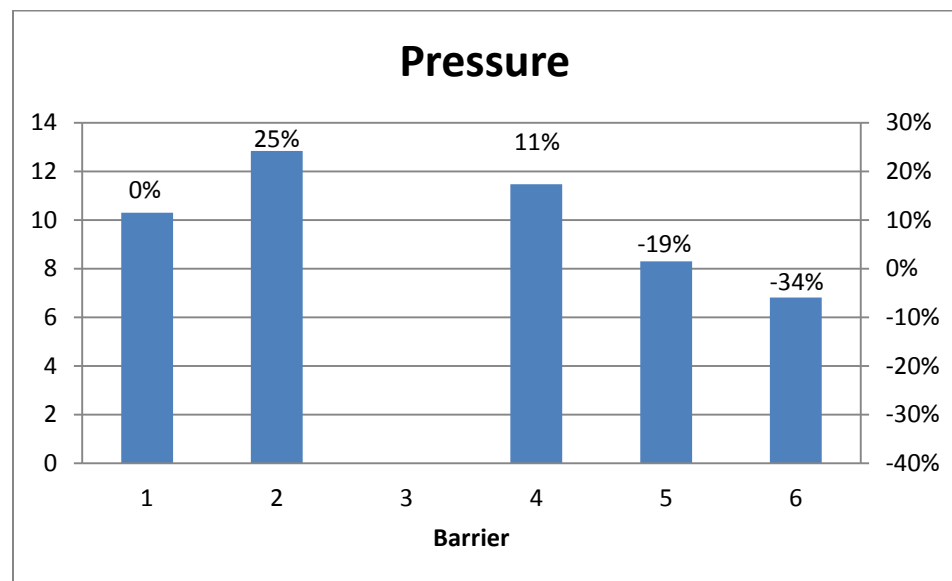


Figure 6.8 Normalized pressure at distance 0.6 m, showing percent pressure difference between the barrier and barrier 1

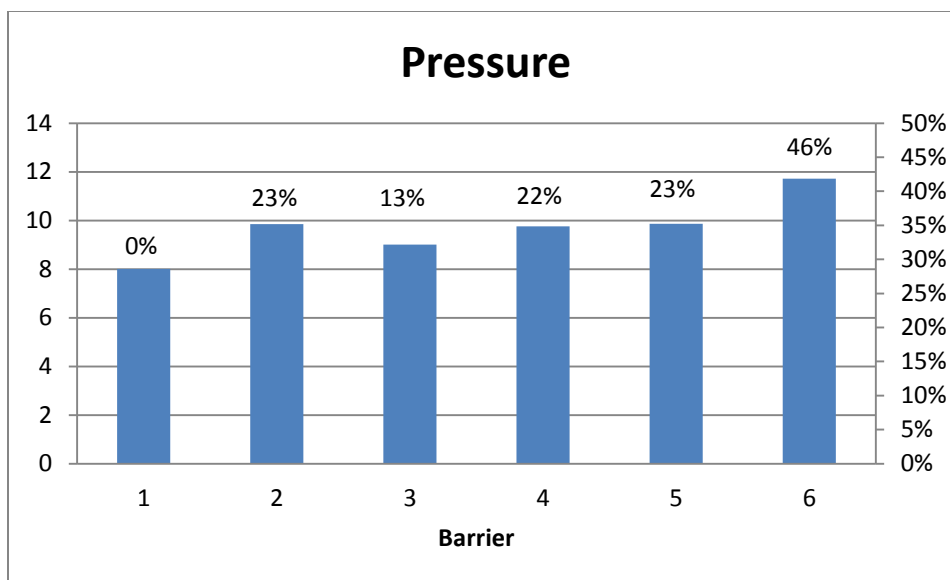


Figure 6.9 Normalized pressure at distance 1.5 m, showing percent pressure difference between the barrier and barrier 1

See Appendix H to examine the data in tabular form. One observation made by the author during testing was that all barriers with a medium (4, 5, 6) showed damage sooner than barriers without a medium (2, 3) and the solid concrete barrier. See Appendix I for pictures of the barriers. It was also observed that on the barriers with media cracking first appeared on the top of the barrier between the PVC pipes used to fill the barrier. Transducer 1, which measured the unaffected pressure, was a baseline and used to normalize the data. The impulse for Barrier 4 was consistently higher than Barrier 1, the control specimen. The pressures for Barrier 4 followed the same trend except at a distance of 0.3 m. It is almost as if the barrier is amplifying the energy from the blast instead of dampening it (Nesterenko, 2003). The impulse on the barriers is a little more chaotic. The impulse increases for some barriers and decreases for others. This could be from the medium reacting differently to the shock wave but it could also be the slight weather differences. The goal here is to reduce the peak pressure, as much as possible,

and extend it over a longer period of time. However, If the pressure is applied long enough it could make the impulse larger. To keep the structural integrity of the building, a low impulse is also desired. Barrier 6, which shows the most potential, has a maximum reduction in pressure of one percent at five feet from the barrier and a maximum reduction in pressure of thirty-four percent at six-hundred-mm. Barrier 6 has the highest percent drop in impulse, twenty-four percent, of any barrier at any distance. Looking at the data in table form all samples taken are very close in value with very few outliers. Some of the barriers increase the pressure, and also the impulse, when compared to a solid concrete barrier. It is unknown if it is the shock passing through the barrier, the reflected wave going over the barrier or different weather conditions that cause this effect. The weather was as constant as possible, kept so by testing on days of similar conditions. But there are still days that have small amounts of wind and others that do not, and this will have some small effect on the blast wave. All barriers are set up in the same manner and in the same position to remove as many variables as possible. The medium fills the interior of the barrier, and is a lower density, except for steel grit which is higher, than the concrete surrounding it. Because of this, the shock wave passes through the medium, reducing the shock wave by crushing the medium. But when it makes contact with the back side of the barrier, the shock is transmitted into the concrete and another shock wave, not a rarefaction, is reflected back into the medium.

7. CONCLUSIONS

It was the author's intent to take three different types of media and use them in such a way to improve a standard concrete barrier. It was not the intent of this research to optimize the system being tested, but to effectively test different media mitigation properties. The author tested three different types of media: pumice, steel grit and foam. These different media were placed inside concrete barriers for testing. The barriers use a newer method of re-enforcement called LCF, instead of rebar, to increase the tensile strength of the surrounding concrete. Using LCF also decreases the overall weight and cost compared to using rebar. Six barriers were constructed and tested to determine how the changes made to the barriers modified the pressure at a fixed standoff behind the barrier. It is shown that soft materials placed in a barrier can mitigate a blast better than a standard concrete barrier. Most of the barriers show an unexpected trend of increasing the peak pressure but decreasing impulse. Barrier 6, which contained steel grit, does not follow this unexpected behavior as the pressure and impulse both show decreases when compared to a solid concrete barrier. This research finds that, of the three media types tested, steel grit is the most efficient means of mitigating blast energy. Barrier 6 shows that it is possible to reduce the pressure by thirty-four percent and reduce the impulse by twenty-four percent. This research will allow future research to take the next step in designing a better blast barrier and testing other media.

8. FUTURE WORK

It is the belief of the author that there is considerable work to be done in this area of study. Future research in this area should take into consideration that the testing done in this paper is limited. There are several areas that need to be expanded and researched. The design of the barrier will have the largest effect on how the blast energy will be directed and should therefore be optimized as much as possible. This is difficult; the barrier not only needs to be very efficient about where the blast energy is directed but also needs to be able to withstand any initial impact and damage done by a vehicle. The next area that could be expanded is the medium itself. Only three different types of media are tested and only one material size. More research may show that there is an optimal size for the medium to absorb a maximum amount of energy.

APPENDIX A
CONCRETE FORMULA SHEET

APPENDIX B

MATLAB CODE FOR EXPLOSIVE PROPERTIES

This is the Matlab code used to bring several calculations together for comparing and contrasting values.

```

clc
clear all
close all

format short
% This first section runs the BEC calculations.
disp('Open Storage/STANDARD')
disp('Bulk/Light Cased: STANDARD')
syms tnt h6 tritonal compb A3 C4 D hbx1 hbx3 minol anfo
disp('tnt, h6, tritonal, compb, A3, C4, D, hbx1, hbx3, minol, anfo')
E = C4%input('Choose an explosive from the list above ');
P = 1.5%input('Enter Total NEW (lbs) ');
A = 1136%input('Enter Altitude (ft) ');
n = .1%input('Enter step size (ft) ');
M = 5%input('Enter max range (ft) ');
Ta = 60%input('Enter ambient Temperature (F) ');
HOB = 1.92%input('Enter height of charge from ground (ft) ');
rc = .16667%input('Enter the charge radius in feet ');
rhox = 1.225%input('Enter the density in kg/m^3 ');%1 kg/m^3 = 1 grams/litre
r = rc +.1:n:M;
Pa = 101325*(1-2.25577*10^-5*A)^5.25588;
Ta = (Ta - 32)*(5/9);%converts to C
k = 1.4;%ratio of specific heats for air
R = 287;%gas constant R = 1716(ft lb/slug Rankin) or R = 286.9 (j/kg K)
AT = Ta + 273.16;%Absoulute Temperature in (K or R)
ax = (k*R*AT)^(1/2);%Speed of sound in (m/s or ft/s)
ax = ax * 3.28;

Z = 0;
while Z < .2
    d = .4%input('Enter Range to object (ft) ');

    % Converts explosive to tnt equivalent weight
    if E == tnt
        W = P;
        w = 1.144714243;
    elseif E == h6
        W = P * 1.35;
        w = 1.265148998;
    elseif E == tritonal
        W = P * 1.07;
        w = 1.170824169;
    elseif E == compb
        W = P * 1.11;
        w = 1.185235759;
    elseif E == A3
        W = P * 1.07;
        w = 1.170824169;
    elseif E == C4
        W = P * 1.3;
        w = 1.249332977;
    elseif E == D
        W = P * 0.92;

```

```

    w = 1.113336282;
elseif E == hbx1
    W = P * 1.17;
    w = 1.206217728;
elseif E == hbx3
    W = P * 1.14;
    w = 1.195818721;
elseif E == minol
    W = P * 1.2;
    w = 1.216440399;
elseif E == anfo
    W = P * 0.83;
    w = 1.075779136;
end
for i = 1 : M/n
    d = d:n:M;
    Z = d / W^(1/3);
    % W^(1/3)
    %difference = (.5 - Z) * 1.5

    if Z < .2
        disp('Increase d')
        %disp('Please add the difference to the distance you entered. Then enter that value as d')
    elseif Z < 2
        disp('Warning some values are out of range')
    end
end
end
Z = transpose(Z);
xlswrite('test.xls',Z,1,'AA2')

for i = 1 : size(Z,2)

%Incident pressure (psi)
if Z(i) < .5
    OP = 0; %Out of Range
elseif Z(i) < 7.25
    OP(i) = exp((((0.0685*log(Z(i))-0.1416)*log(Z(i))-0.2815)*log(Z(i))-1.4398)*log(Z(i))+6.9137);
elseif Z(i) < 60
    OP(i) = exp((((-0.0127*log(Z(i))+0.0733)*log(Z(i))+0.2709)*log(Z(i))-3.7001)*log(Z(i))+8.8035);
elseif Z(i) <= 5000
    OP(i) = exp(-1.4066*log(Z(i))+5.42327);
elseif Z(i) > 5000
    OP = 0; %Out of Range
end

%Altitude correction
if A < 51
    if A > 14.696
        J24 = 14.696;
    elseif A < 8
        J24 = 14.696;
    else
        J24 = A;
    end
end
else

```

```

    J24 = 14.72454 * exp(-0.00003758989 * A);
end
Sp = J24 / 14.696;
if OP == 0
    OPA = 0;
else
    OPA = Sp * OP;
end

%Reflected Pressure (psi)
if Z(i) < .3
    RP(i) = 0; %Out of Range
elseif Z(i) < 4
    RP(i) = exp(((((-0.0118*log(Z(i))+0.0696)*log(Z(i))-0.0128)*log(Z(i))-0.2199)*log(Z(i))-
0.2877)*log(Z(i))-1.7511)*log(Z(i))+9.0795);
elseif Z(i) <= 100
    RP(i) = exp(((((-0.008181*log(Z(i))+0.16333)*log(Z(i))-1.33455)*log(Z(i))+5.56754)*log(Z(i))-
11.85735)*log(Z(i))+9.15826)*log(Z(i))+5.1515);
elseif Z(i) <= 500
    RP(i) = 2 * OP(i);
elseif Z(i) > 500
    RP(i) = 0; %Out of Range
end

%Altitude correction
if A < 51
    if A > 14.696
        J24 = 14.696;
    elseif A < 8
        J24 = 14.696;
    else
        J24 = A;
    end
else
    J24 = 14.72454 * exp(-0.00003758989 * A);
end
Sp = J24 / 14.696;
if RP == 0
    RPA = 0;
else
    RPA = Sp * RP;
end

%Time of arrival (ms)    %%%% need to figure out how to calculate w %%%%
if Z(i) < .2
    ta1(i) = 0; %Out of Range
elseif Z(i) < 4.5
    ta1(i) = w*exp(((((-
0.008615*log(Z(i))+0.003656)*log(Z(i))+0.01825)*log(Z(i))+0.1313)*log(Z(i))+1.5348)*log(Z(i))-
2.5671);
elseif Z(i) <= 100
    ta1(i) = w*exp(((((-0.0081529*log(Z(i))+0.13045)*log(Z(i))-0.78101)*log(Z(i))+2.01409)*log(Z(i))-
0.44021)*log(Z(i))-1.79097);
elseif Z(i) <= 500
    ta1(i) = w*0.6559951*(exp(log(Z(i))))^1.0478
elseif Z(i) > 500

```



```

    ta1(i) = 0; %Out of Range
end

%Altitude correction
J26 = AT;
if A < 51
    if A > 14.696
        J24 = 14.696;
    elseif A < 8
        J24 = 14.696;
    else
        J24 = A;
    end
else
    J24 = 14.72454 * exp(-0.00003758989 * A);
end
St = ((14.696 / J24)^(1/3)) * ((288.16 / J26)^(1/2));
if ta1 == 0
    ta1A = 0;
else
    ta1A = St * ta1;
end

%Positive phase duration (ms)
if Z(i) < .5
    PPD(i) = 0; %Out of Range
elseif Z(i) < 2.5
    PPD(i) = w*exp(((((-0.608*log(Z(i))-
0.05773)*log(Z(i))+1.1249)*log(Z(i))+1.3552)*log(Z(i))+0.45)*log(Z(i))-1.7221);
elseif Z(i) < 7
    PPD(i) = w*exp((((0.8817*log(Z(i))-8.3256)*log(Z(i))+32.0236)*log(Z(i))-
60.4348)*log(Z(i))+55.0513)*log(Z(i))-18.7701);
elseif Z(i) <= 100
    PPD(i) = w*exp((((0.02624*log(Z(i))-0.4647)*log(Z(i))+3.2552)*log(Z(i))-
11.2975)*log(Z(i))+19.7805)*log(Z(i))-13.0597);
elseif Z(i) <= 500
    PPD(i) = 1.0029*w*exp(-0.044686+0.51213*log(Z(i))-0.02895*(log(Z(i)))^2);
elseif Z(i) > 500
    PPD(i) = 0; %Out of Range
end

%Altitude correction
J26 = AT;
if A < 51
    if A > 14.696
        J24 = 14.696;
    elseif A < 8
        J24 = 14.696;
    else
        J24 = A;
    end
else
    J24 = 14.72454 * exp(-0.00003758989 * A);
end
St = ((14.696 / J24)^(1/3)) * ((288.16 / J26)^(1/2));
if PPD == 0

```

```

    PPDA = 0;
else
    PPDA = St * PPD;
end

%Positive phase impulse (psi-ms)
if Z(i) < .5
    PPI(i) = 0; %Out of Range
elseif Z(i) < 2.41
    PPI(i) = w*exp((((-0.087*log(Z(i))+0.03)*log(Z(i))+0.963*log(Z(i))-0.466)*log(Z(i))+2.975);
elseif Z(i) < 6
    PPI(i) = w*exp((((-0.432*log(Z(i))+2.96)*log(Z(i))-7.459)*log(Z(i))+7.26)*log(Z(i))+0.911);
elseif Z(i) < 85
    PPI(i) = w*exp((((-0.00554*log(Z(i))+0.0793)*log(Z(i))-
0.4416)*log(Z(i))+0.1633)*log(Z(i))+3.2484);
elseif Z(i) <= 1000
    PPI(i) = w*exp(-1.062*log(Z(i))+4.7702);
elseif Z(i) > 1000
    PPI(i) = 0; %Out of Range
end

%Altitude correction
J26 = AT;
if A < 51
    if A > 14.696
        J24 = 14.696;
    elseif A < 8
        J24 = 14.696;
    else
        J24 = A;
    end
else
    J24 = 14.72454 * exp(-0.00003758989 * A);
end
Si = ((J24 / 14.696)^(2/3)) * ((288.16 / J26)^(1/2));
if PPI == 0
    PPIA = 0;
else
    PPIA = Si * PPI;
end

%Reflected impulse (psi-ms)
if Z(i) < .2
    RI(i) = 0; %Out of Range
elseif Z(i) <= 100
    RI(i) = w*exp((((-0.01123*log(Z(i))+0.1322)*log(Z(i))-1.5622)*log(Z(i))+5.9313);
elseif Z(i) > 100
    RI(i) = 0; %Out of Range
end

%Altitude correction
J26 = AT;
if A < 51
    if A > 14.696
        J24 = 14.696;
    elseif A < 8

```

```

        J24 = 14.696;
    else
        J24 = A;
    end
end
else
    J24 = 14.72454 * exp(-0.00003758989 * A);
end
Si = ((J24 / 14.696)^(2/3)) * ((288.16 / J26)^(1/2));
if RI == 0
    RIA = 0;
else
    RIA = Si * RI;
end

%Dynamic overpressure (psi)
if Z(i) < .5
    DO(i) = 0; %Out of Range
elseif Z(i) <= 100
    DO(i) = exp(8.01662-1.80686*(log(Z(i)))-0.424622*(log(Z(i)))^2-
0.393993*(log(Z(i)))^3+0.189752*(log(Z(i)))^4-0.0209928*(log(Z(i)))^5);
elseif Z(i) > 100
    DO(i) = 0; %Out of Range
end

%Altitude correction
if A < 51
    if A > 14.696
        J24 = 14.696;
    elseif A < 8
        J24 = 14.696;
    else
        J24 = A;
    end
else
    J24 = 14.72454 * exp(-0.00003758989 * A);
end
Sp = J24 / 14.696;
if DO == 0
    DOA = 0;
else
    DOA = Sp * DO;
end

%Dynamic overpressure impulse (psi-ms)
if Z(i) < .5
    DOI(i) = 0; %Out of Range
elseif Z(i) < 6
    DOI(i) = w*exp(5.02669-1.4977*(log(Z(i)))+0.382073*(log(Z(i)))^2-
2.91667*(log(Z(i)))^3+0.0986917*(log(Z(i)))^4+4.11776*(log(Z(i)))^5-
2.92807*(log(Z(i)))^6+0.584571*(log(Z(i)))^7);
elseif Z(i) <= 100
    DOI(i) = w*exp(-43.5759+106.513*(log(Z(i)))-96.6174*(log(Z(i)))^2+44.3327*(log(Z(i)))^3-
11.1537*(log(Z(i)))^4+1.46535*(log(Z(i)))^5-0.0787675*(log(Z(i)))^6);
elseif Z(i) > 100
    DOI(i) = 0; %Out of Range
end

```

```

%Altitude correction
J26 = AT;
if A < 51
    if A > 14.696
        J24 = 14.696;
    elseif A < 8
        J24 = 14.696;
    else
        J24 = A;
    end
else
    J24 = 14.72454 * exp(-0.00003758989 * A);
end
Si = ((J24 / 14.696)^(2/3)) * ((288.16 / J26)^(1/2));
if DOI == 0
    DOIA = 0;
else
    DOIA = Si * DOI;
end
end
OP = transpose(OP);
xlswrite('test.xls',OP,1,'A2')
OPA = transpose(OPA);
xlswrite('test.xls',OPA,1,'B2')
RP = transpose(RP);
xlswrite('test.xls',RP,1,'D2')
RPA = transpose(RPA);
xlswrite('test.xls',RPA,1,'E2')
ta1 = transpose(ta1);
xlswrite('test.xls',ta1,1,'G2')
ta1A = transpose(ta1A);
xlswrite('test.xls',ta1A,1,'H2')
PPD = transpose(PPD);
xlswrite('test.xls',PPD,1,'J2')
PPDA = transpose(PPDA);
xlswrite('test.xls',PPDA,1,'K2')
PPI = transpose(PPI);
xlswrite('test.xls',PPI,1,'M2')
PPIA = transpose(PPIA);
xlswrite('test.xls',PPIA,1,'N2')
RI = transpose(RI);
xlswrite('test.xls',RI,1,'O2')
RIA = transpose(RIA);
xlswrite('test.xls',RIA,1,'P2')
DO = transpose(DO);
xlswrite('test.xls',DO,1,'Q2')
DOA = transpose(DOA);
xlswrite('test.xls',DOA,1,'R2')
DOI = transpose(DOI);
xlswrite('test.xls',DOI,1,'S2')
DOIA = transpose(DOIA);
xlswrite('test.xls',DOIA,1,'T2')

```


APPENDIX C

TRANSDUCER SPECIFICATION SHEET

Product specifications for the transducers used in this research.

Product Specifications

	ENGLISH	SI	
Performance			
Measurement Range (for $\pm 5V$ output)	200 psi	1379 kPa	
Useful Overrange (for $\pm 10V$ output)	400 psi	2758 kPa	[2]
Sensitivity (± 5 mV/psi)	25 mV/psi	3.6 mV/kPa	
Maximum Pressure (static)	1000 psi	6895 kPa	
Resolution	0.001 psi	0.007 kPa	[3]
Resonant Frequency	≥ 500 kHz	≥ 500 kHz	
Rise Time (Reflected)	≤ 1.0 μ sec	≤ 1.0 μ sec	
Low Frequency Response (-5 %)	0.5 Hz	0.5 Hz	
Nonlinearity	≤ 1.0 % FS	≤ 1.0 % FS	[1]
Environmental			
Acceleration Sensitivity	≤ 0.002 psi/g	≤ 0.0014 kPa/(m/s ²)	
Temperature Range (Operating)	-100 to +275 °F	-73 to +135 °C	
Temperature Coefficient of Sensitivity	≤ 0.03 %/°F	≤ 0.054 %/°C	[3]
Maximum Flash Temperature	3000 °F	1650 °C	
Maximum Shock	20000 g pk	196000 m/s ² pk	
Electrical			
Output Polarity (Positive Pressure)	Positive	Positive	
Discharge Time Constant (at room temp)	≥ 1.0 sec	≥ 1.0 sec	
Excitation Voltage	20 to 30 VDC	20 to 30 VDC	
Constant Current Excitation	2 to 20 mA	2 to 20 mA	
Output Impedance	<100 Ohm	<100 Ohm	
Output Bias Voltage	8 to 14 VDC	8 to 14 VDC	
Electrical Isolation	100000000 Ohm	100000000 Ohm	
Physical			
Sensing Geometry	Compression	Compression	
Sensing Element	Quartz	Quartz	
Housing Material	Stainless Steel	Stainless Steel	
Diaphragm	Invar	Invar	
Sealing	Welded Hermetic	Welded Hermetic	
Electrical Connector	10-32 Coaxial Jack	10-32 Coaxial Jack	
Weight	0.41 oz	11.6 gm	

APPENDIX D

TEST SETUP MATRIX

The test matrix used to keep track of distances, errors, and other information.

Test	Barrier	Standoff (ft)	Charge size (lb)	Transducer error	Distance from charge to transducer (ft)	Distance of transducer 1 To front of barrier (ft)	Distance of transducer 2 To front of barrier (ft)
1	N/A	5	1.5	N	10	15	5
2	N/A	5	1.5	N	10	15	5
3	N/A	5	1.5	N	10	15	5
4	N/A	2	0.5	N	7	9	5
5	N/A	2	0.5	N	7	9	5
6	N/A	2	0.5	N	7	9	5
7	N/A	1	0.5	N	6	7	5
8	N/A	1	0.5	N	6	7	5
9	N/A	1	0.5	N	6	7	5
10	B1	5	1.5	N	10	15	5
11	B1	5	1.5	N	10	15	5
12	B1	5	1.5	N	10	15	5
13	B1	2	1.5	N	7	9	5
14	B1	2	1.5	N	7	9	5
15	B1	2	1.5	N	7	9	5
16	B1	1	1.5	N	6	7	5
17	B1	1	1.5	N	6	7	5
18	B1	1	1.5	N	6	7	5
19	B2	5	1.5	N	10	15	5
20	B2	5	1.5	N	10	15	5
21	B2	5	1.5	N	10	15	5
22	B2	2	1.5	N	7	9	5
23	B2	2	1.5	Y	7	9	5
24	B2	2	1.5	Y	7	9	5
25	B2	1	1.5	Y	6	7	5
26	B2	1	1.5	Y	6	7	5
27	B2	1	1.5	Y	6	7	5
28	B3	5	1.5	N	10	15	5
29	B3	5	1.5	N	10	15	5
30	B3	5	1.5	N	10	15	5
31	B3	2	1.5	Y	7	9	5
32	B3	2	1.5	Y	7	9	5
33	B3	2	1.5	Y	7	9	5
34	B3	1	1.5	Y	6	7	5
35	B3	1	1.5	Y	6	7	5
36	B3	1	1.5	Y	6	7	5
37	B4	5	1.5	N	10	15	5
38	B4	5	1.5	N	10	15	5
39	B4	5	1.5	N	10	15	5
40	B4	2	1.5	N	7	9	5
41	B4	2	1.5	Y	7	9	5
42	B4	2	1.5	N	7	9	5
43	B4	1	1.5	N	6	7	5
44	B4	1	1.5	N	6	7	5
45	B4	1	1.5	N	6	7	5
46	B5	5	1.5	N	10	15	5
47	B5	5	1.5	N	10	15	5
48	B5	5	1.5	N	10	15	5
49	B5	2	1.5	N	7	9	5
50	B5	2	1.5	N	7	9	5
51	B5	2	1.5	N	7	9	5
52	B5	1	1.5	N	6	7	5
53	B5	1	1.5	Y	6	7	5
54	B5	1	1.5	N	6	7	5
55	B6	5	1.5	N	10	15	5
56	B6	5	1.5	N	10	15	5
57	B6	5	1.5	N	10	15	5
58	B6	2	1.5	N	7	9	5
59	B6	2	1.5	N	7	9	5
60	B6	2	1.5	N	7	9	5
61	B6	1	1.5	N	6	7	5
62	B6	1	1.5	Y	6	7	5
63	B6	1	1.5	N	6	7	5

APPENDIX E

STEP-BY-STEP PROCESS TO CALIBRATE DAS

These are step-by-step instructions for setting up the DAS and using it during testing.

The Synergy Version 5.0

First, unpack the Synergy data acquisition system and set it on a table where it will be protected from the blast. Next, plug in the power cord, mouse and key board, the mouse and key board plug into a USB connection. Turn the power on and wait for the data acquisition system to boot up. Once the data acquisition system screen shows the desktop find the Synergy software icon and double click it to open the program. For a picture of the main menu see the Figure below.

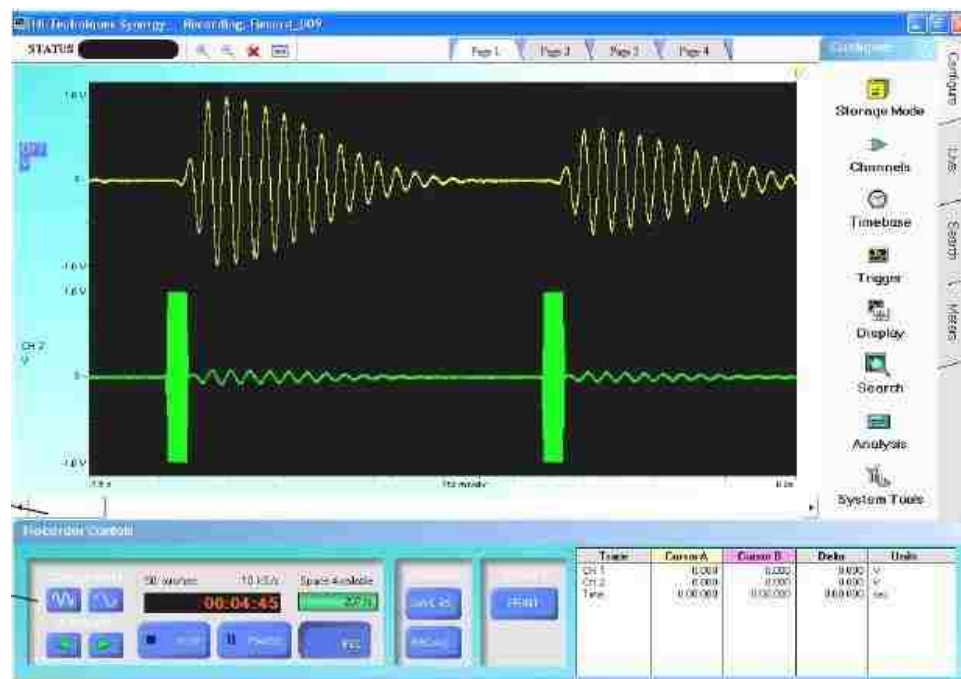


Figure 9.1 Main menu for Synergy recording program.

1. The first step in the program is to open system tools and restore the system to factory default values see Figure below. This insures that settings from the last use won't affect this experiment.

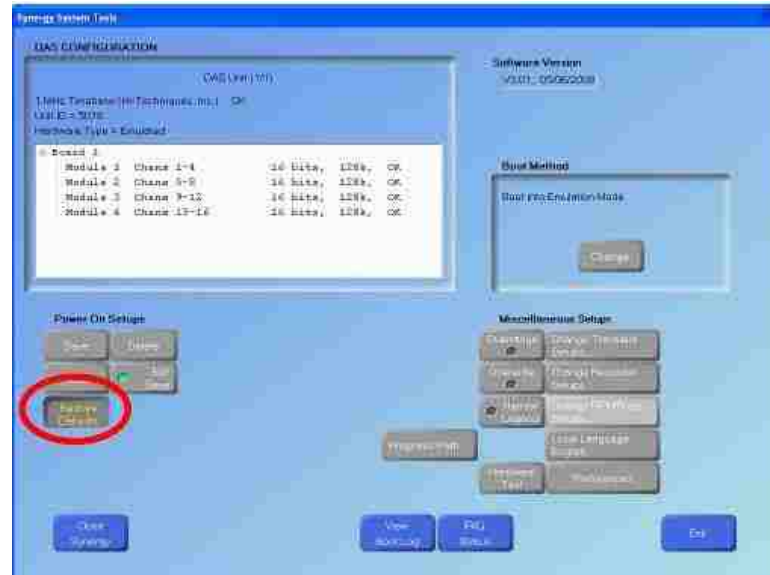


Figure 9.2 Menu for restoring defaults.

- Next click storage mode and select scope mode not recorder, while in this menu check the save all sweeps to disk box and click the Recorder storage settings button see Figure below. In this menu under Data Format set the type of files to be saved, the first should be left to the default file type which is a .syn file; the second should be changed to a .csv file type see Figure below.

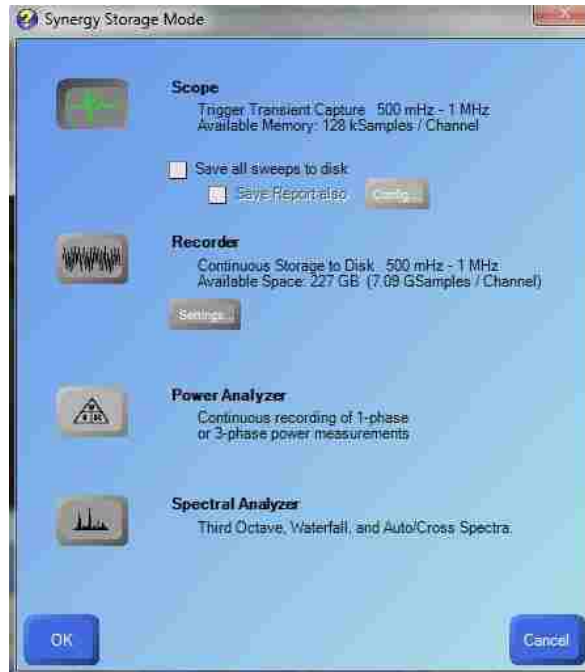


Figure 9.3 Synergy storage mode menu.

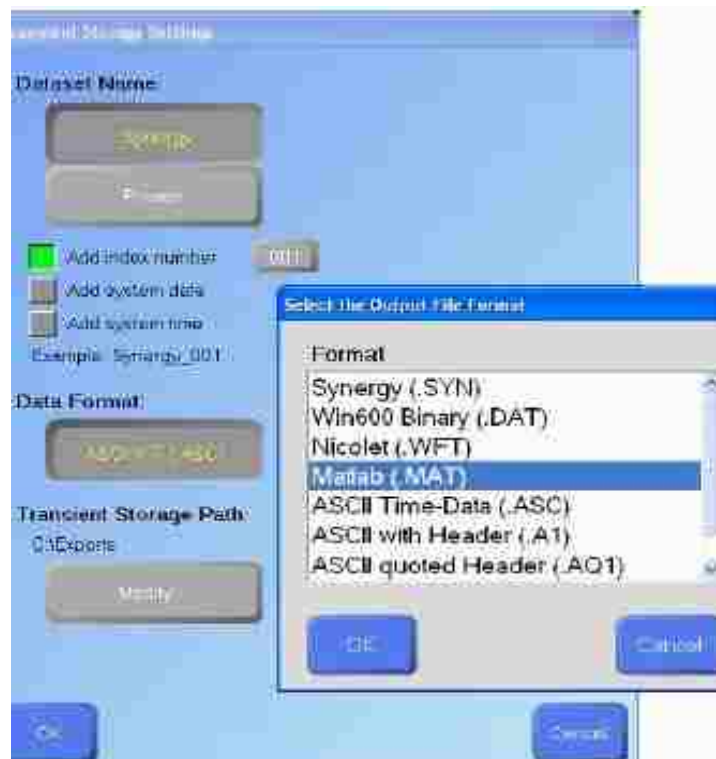


Figure 9.4 Storage settings menu.

- Now set up and calibrate the channels being used. Under channels a spread sheet opens, check channel one, two and three are on and make sure all other channels are not checked. Only these three channels will be used. For channels one and two under mode change the block from Diff DC to IEPE. For channel three leave the mode as DC because this will be the trigger for the DAS. Range will be auto scaled and the default sample rate is set to 1 MS/s. This can be changed if desired see the Figure below.

Channel	Name	On	Mode	Range	Bias	Filter Type	Filter Freq.
CH1	CH 1	<input checked="" type="checkbox"/>	IEPE	3.00 ps	0.00 psf	OH	
CH2	CH 2	<input type="checkbox"/>	Diff DC	3.97 ps	0.00 psf	OH	
CH3	CH 3	<input type="checkbox"/>	Diff DC	3.95 ps	0.00 psf	OH	
CH4	CH 4	<input type="checkbox"/>	Diff DC	2.03 ps	0.00 psf	OH	
CH5	CH 5	<input type="checkbox"/>	Diff DC	4.01 psf	0.00 psf	OH	
CH6	CH 6	<input type="checkbox"/>	Diff DC	20.0 mV	0.00 V	OH	
CH7	CH 7	<input type="checkbox"/>	Diff DC	20.0 mV	0.00 V	OH	
CH8	CH 8	<input type="checkbox"/>	Diff DC	20.0 mV	0.00 V	OH	
CH9	CH 9	<input type="checkbox"/>	Diff DC	20.0 mV	0.00 V	OH	
CH10	CH 10	<input type="checkbox"/>	Diff DC	20.0 mV	0.00 V	OH	
CH11	CH 11	<input type="checkbox"/>	Diff DC	20.0 mV	0.00 V	OH	
CH12	CH 12	<input type="checkbox"/>	Diff DC	20.0 mV	0.00 V	OH	

Figure 9.5 Main menu for Synergy recording program.

- While still under the channels window click the button calibration wizard at the top. This brings up a new window.
- Click the button labeled Enter information from data sheet then click next; see the Figure below.



Figure 9.6 Calibration Wizard menu 1.

6. At the top of the next page after the words “Physical Units you are measuring” is a white box. Enter the unit “psi” in this box see the Figure below. Then select the unit mV/psi and click next.

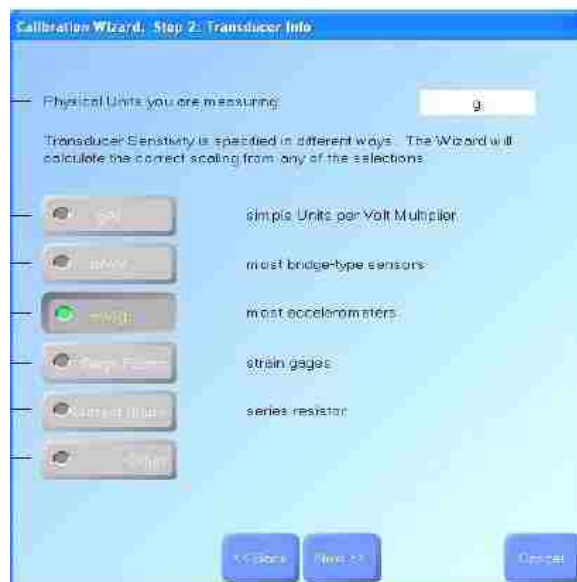


Figure 9.7 Calibration Wizard menu 2 units.

- The next window asks for Sensitivity in mV/psi. This number is found on the case the transducer can be seen in the Figure below.

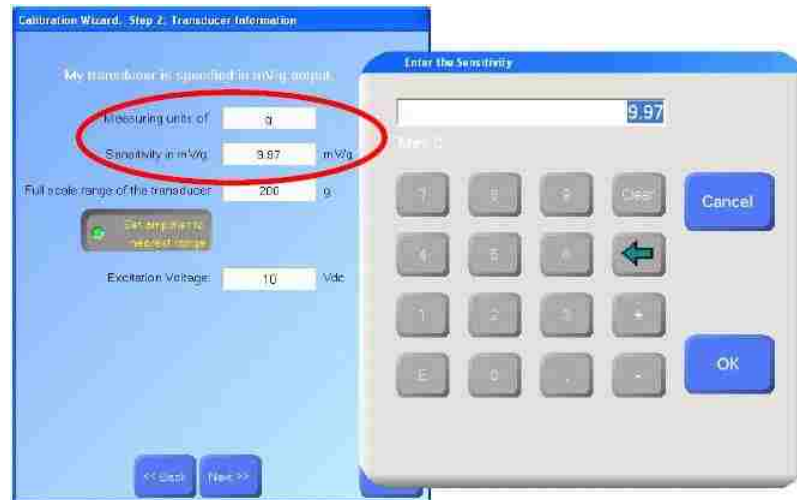


Figure 9.8 Calibration Wizard menu 3 calibration.

- Under the sensitivity it asks for the Full scale range of the transducer. For our experiment enter the value 1000 psi. This is the measuring value of the transducer. Click next.
- The next window gives a summary see the Figure below. Check that the summary is correct and click finish

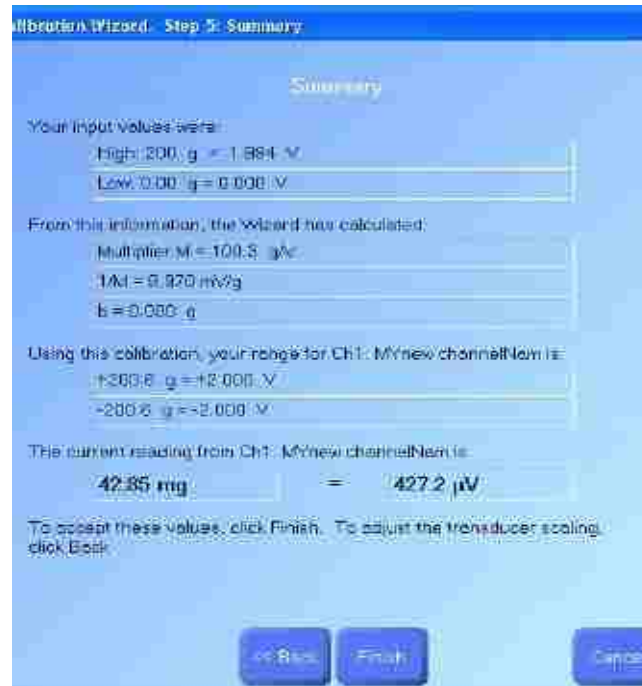


Figure 9.9 Calibration Wizard menu 4.

10. Click the button labeled Display. In this window check the box labeled Auto scale Tracers. Then click OK.
11. The data acquisition system has now been calibrated for operation and a line run for the trigger. The data acquisition system is ready for activation of the shot.
12. Along the top of the screen select “ALL” to center the readings and drag the selection bars in to isolate the trace.
13. Use the Waveform Calculator and the selection bars at the top of the screen to determine the pressures and time differences on the selected area.
14. Click the button labeled SAVE AS. In this window select the following options.
 - Displayed Traces
 - Between Cursors

Then change the file path using the button labeled Change. Once the file is set click save.

15. Click the button labeled Exit. This returns the data acquisition system to the main menu and is ready for the next run.
16. Repeat steps 11 – 14 for each shot see Figure 3. to locate labels.

APPENDIX F

WEATHER CONDITIONS FOR TEST DAYS

These are the weather conditions for the days that testing occurred.

Barrier	1	1	1	2	3	4	5	6
Test day	7/8/2013	7/9/2013	7/10/2013	7/12/2013	7/16/2013	7/24/2013	7/25/2013	8/1/2013
Temperature (F)	91.4	97.9	85.7	89.3	92.9	86	85.9	79
Relative humidity (%)	54.2	49.2	71.1	38	52.7	53	46.3	76.1
Barometric pressure (mBAR)	985.6	984.4	981.3	985.1	991	981.3	984.8	984.2
Altitude (ft)	1100	1100	1100	1100	1100	1100	1100	1100
Dew point (F)	72.1	72.1	75.9	59	76	66.1	63	69.4
Average wind speed (miles/hour)	5.7	2	2.25	2.25	3	1.5	0.6	0

Figure 9.12 Weather conditions for test days

APPENDIX G

STEP-BY-STEP PROCESS TO CALCULATE IMPULSE

This is a step-by-step process for calculating the impulse using the DAS.

1. Open synergy software and load desired test file by pressing recall button at bottom of screen. See figure below.

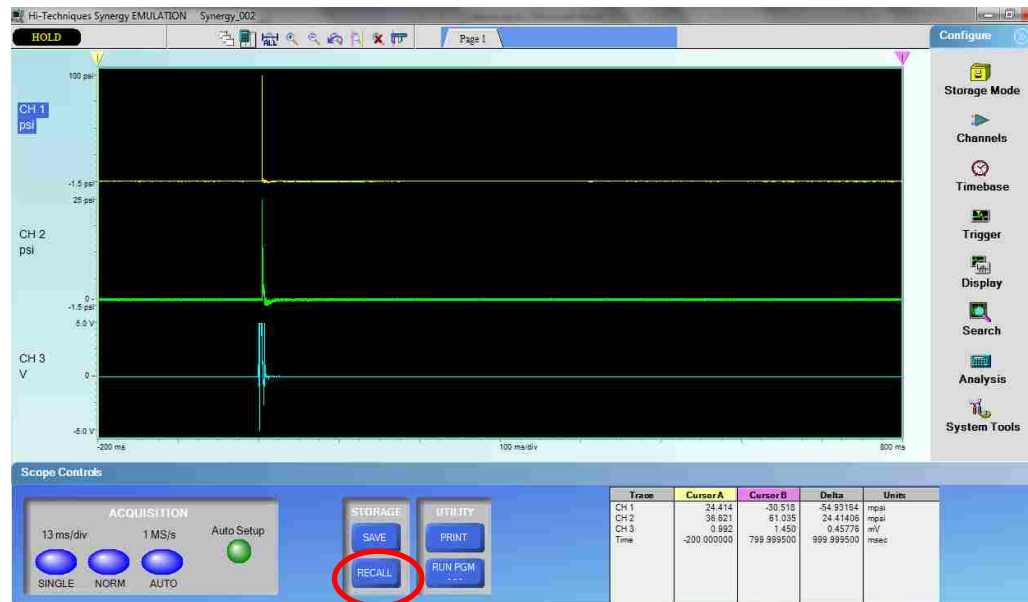


Figure 9.13 Main menu of synergy software

2. Once the file is loaded one channel has to be focused on at a time. Working on channel one move the yellow vertical line closer but to the left of the pressure spike. Then move the pink vertical line closer but to the right of the pressure spike.

- Click zoom button on top of screen circled in figure below. The zoom can be used to get closer or further away as needed. See figure below.

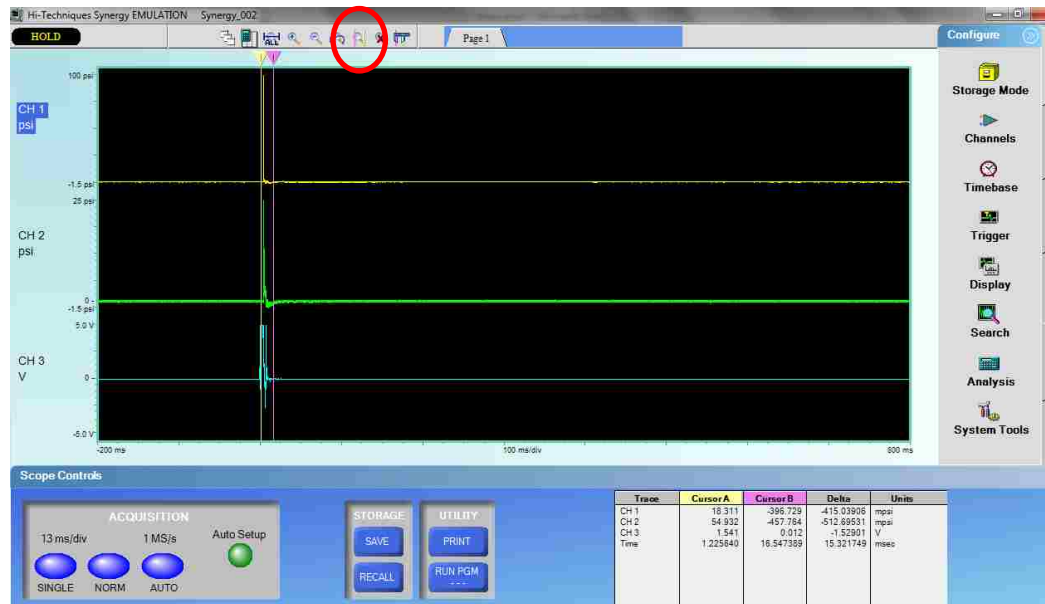


Figure 9.14 Move cursers and zoom

- Move yellow vertical line to the base of the left of the pressure spike to the spot closest to zero psi. Next move the pink vertical line coming off the right side of the pressure spike until the curve drops below zero. See figure below.

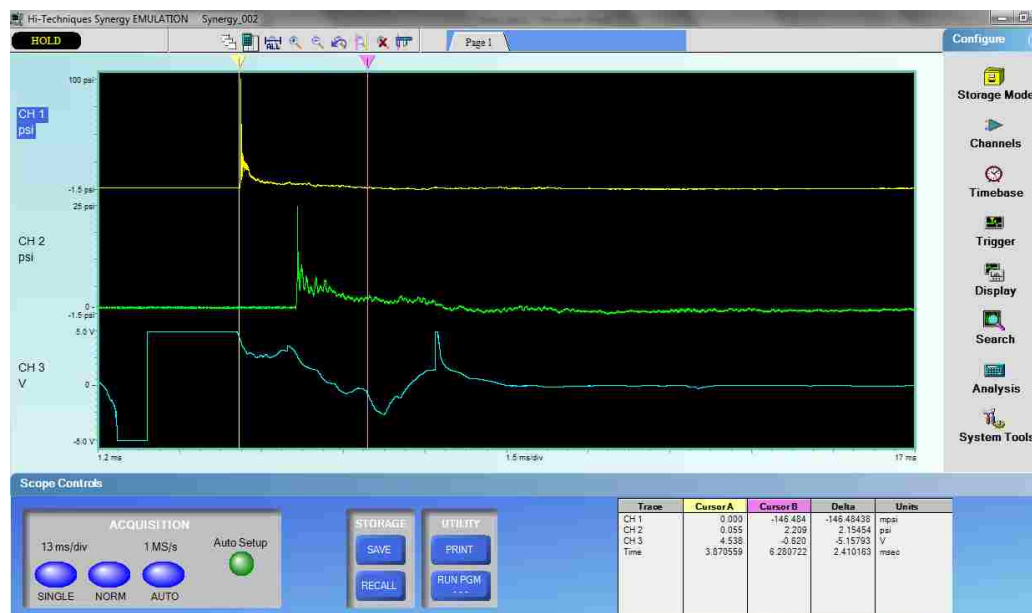


Figure 9.15 Zoom and adjust cursers as needed

- Once the lines are where they need to be click the button on the right side of the screen labeled Analysis. This brings up a new menu window see figure below.

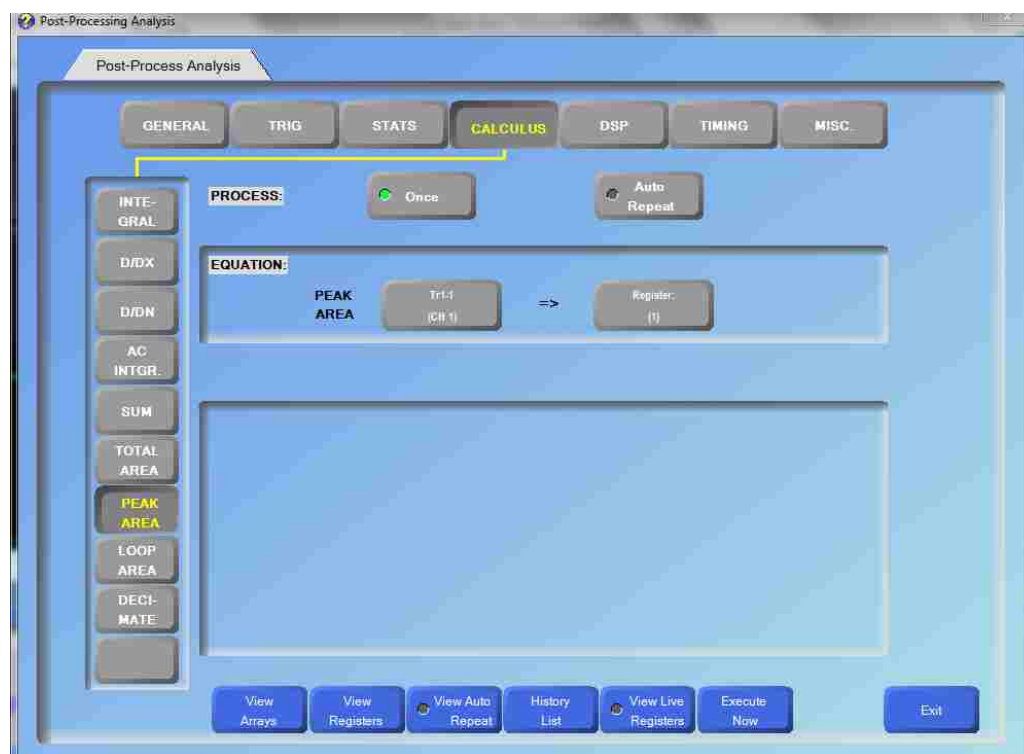


Figure 9.16 Analysis window

6. Select calculus. Then click the button peak area on the left side of the screen. If not already select TR1-1. Directly below that under waveform inputs select the button that says Trace. This brings up a new window see figure below. In this menu select the channel desired.

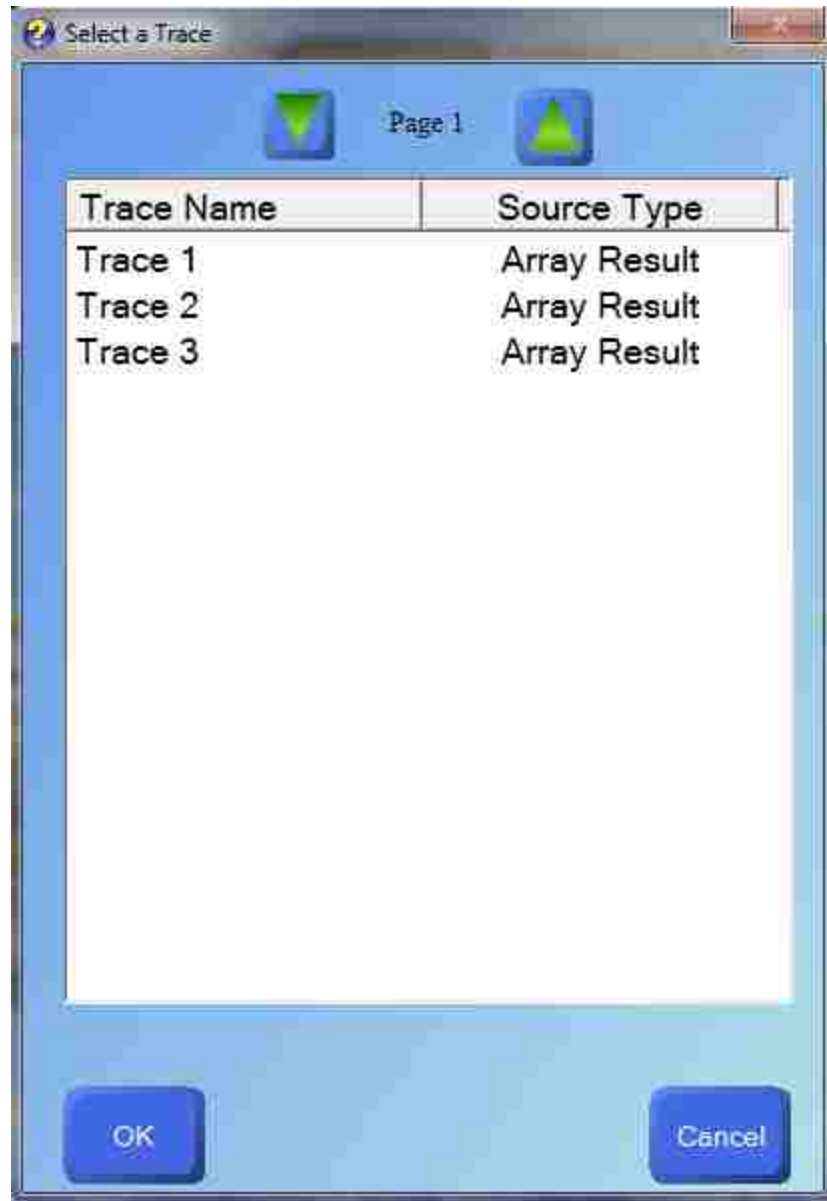


Figure 9.17 Trace window

7. Under samples select between cursors. Then select button under scalar inputs labeled register. This brings up a new window, see figure below.

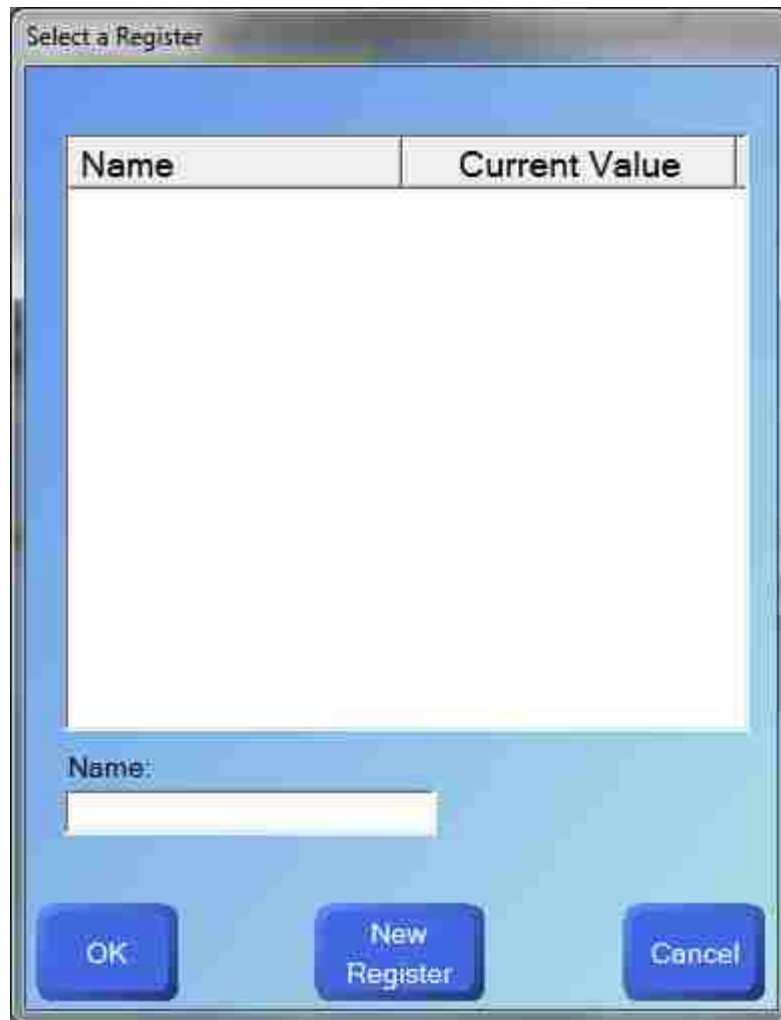


Figure 9.18 Window for register name

8. Select new register button and name the new register. Then select the enter button. The value given is the area under the curve between the vertical yellow and pink

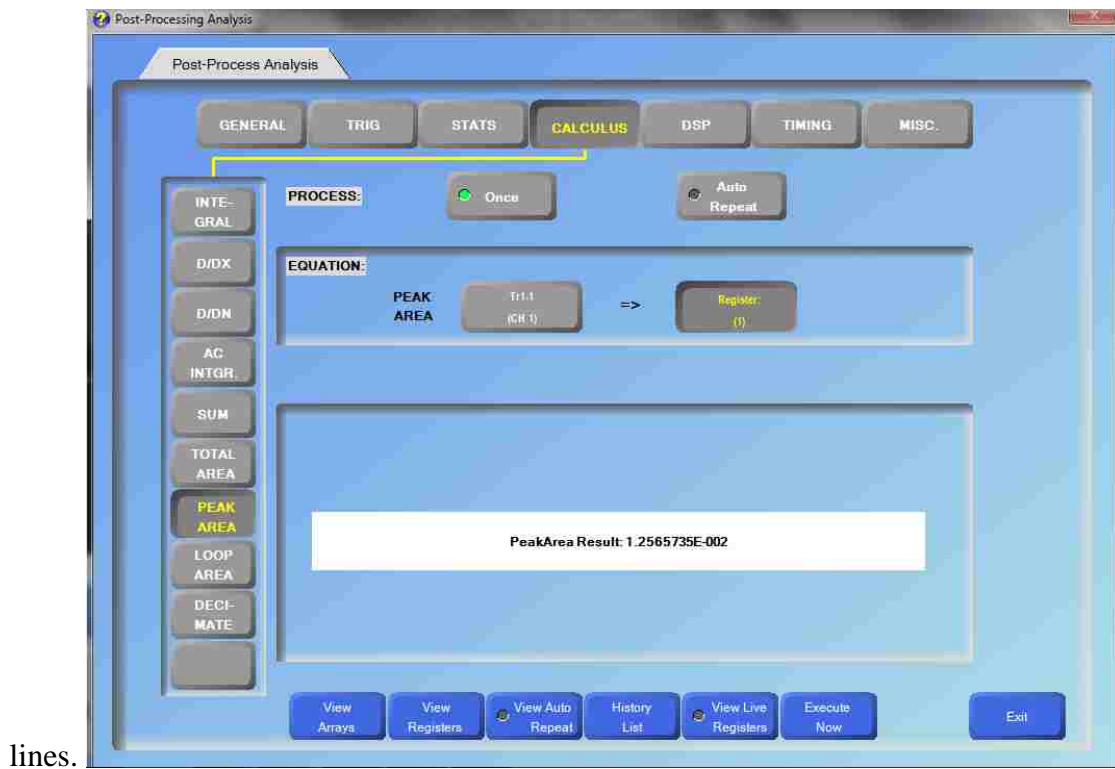


Figure 9.19 Impulse calculation

9. To repeat, repeat steps 2 through 8. Do this for both channels for all tests done.

APPENDIX H
TEST VALUES

These are the numbers pulled from each test before they were averaged.

Impulse	B1		B2		B3		B4		B5		B6	
distance (m)	CH 1 (kPa-ms)	CH 2 (kPa-ms)	CH 1 (kPa-ms)	CH 2 (kPa-ms)	CH 1 (kPa-ms)	CH 2 (kPa-ms)	CH 1 (kPa-ms)	CH 2 (kPa-ms)	CH 1 (kPa-ms)	CH 2 (kPa-ms)	CH 1 (kPa-ms)	CH 2 (kPa-ms)
0.3	222.0111847	75.84233019	0	0	0	0	201.3269129	82.87498263	0	78.60023311	233.7322721	66.25861756
0.3	209.6006216	75.84233019	0	0	0	0	228.905942	84.11603894	250.9691654	82.73708748	234.4217479	57.77806609
0.3	204.0848158	76.53180592	0	0	0	0	230.2848935	83.42656321	262.000777	84.80551467	195.1216313	57.22648551
0.6	197.8795342	70.32652436	0	0	0	0	199.9479614	88.25289331	234.4217479	76.53180592	173.058408	55.15805832
0.6	190.2953012	75.84233019	0	0	0	0	0	77.22128165	227.5269906	80.66866029	113.7634953	51.02120395
0.6	173.058408	71.01600009	197.1900585	63.63860979	0	0	157.8899419	75.84233019	144.7899031	76.53180592	144.7899031	46.19487384
1.5	110.3161166	71.70547582	97.90555352	58.60543697	99.28450498	51.71067968	84.80551467	56.53700978	101.3529322	57.91596124	82.73708748	49.64225249
1.5	115.1424467	75.84233019	96.52660206	56.53700978	99.28450498	53.22752628	86.87394185	57.91596124	96.52660206	58.60543697	79.28970884	48.95277676
1.5	56.53700978	39.30011655	0	64.1212428	93.07922342	54.67542531	84.11603894	64.1212428	104.8003108	59.29491269	83.42656321	53.84805443
1.5	0	0	0	0	97.90555352	52.74489327	0	0	0	0	0	0
Averages												
0.3 (m)	211.898874	76.07215543	0	0	0	0	220.1725828	83.47252826	256.4849712	82.04761175	221.0918838	60.42105638
0.6 (m)	187.0774748	72.39495155	197.1900585	63.63860979	0	0	178.9189517	80.43883505	202.2462138	77.91075738	143.8706021	50.7913787
1.5 (m)	93.99852439	62.28264085	97.21607779	59.75456318	97.38844672	53.08963113	85.26516515	59.52473794	100.8932817	58.60543697	81.81778651	50.81436123

Figure 9.10 Impulse values calculated by DAS computer in kPa-ms

Impulse	B1		B2		B3		B4		B5		B6	
distance (m)	CH 1 (kPa-ms)	CH 2 (kPa-ms)	CH 1 (kPa-ms)	CH 2 (kPa-ms)	CH 1 (kPa-ms)	CH 2 (kPa-ms)	CH 1 (kPa-ms)	CH 2 (kPa-ms)	CH 1 (kPa-ms)	CH 2 (kPa-ms)	CH 1 (kPa-ms)	CH 2 (kPa-ms)
0.3	1705.073478	200.7753323	0	0	0	0	1789.878992	205.8774527	0	176.0921012	0	0
0.3	1566.488856	205.3948197	0	0	0	0	1669.910216	177.6778954	1918.121478	182.6421206	1409.977866	118.658773
0.3	1616.131109	203.8779731	0	0	0	0	1680.941827	183.7452818	1918.121478	230.0091032	1409.977866	141.5493672
0.6	1409.28839	158.2346798	0	0	0	0	2082.216702	184.0900196	2033.953401	156.0283575	1409.977866	120.589305
0.6	1409.977866	138.3777788	0	0	0	0	0	159.4757361	2089.800935	201.8095459	1409.977866	80.73760787
0.6	1409.28839	138.7914642	1409.28839	180.9873789	0	0	1400.325206	255.38181	2213.21709	168.2320779	1409.28839	86.80499428
1.5	1170.040312	58.86054298	1190.035108	95.1476506	1017.666176	70.25757679	769.4549136	99.90503313	1119.019108	189.8126682	774.9707194	59.41901833
1.5	1034.213594	115.9698176	1161.077128	142.9972662	1034.903069	143.8246371	857.7078069	68.12020203	959.060739	57.65396046	765.3180592	50.4144653
1.5	1232.782603	126.4498487	1198.998293	111.6950681	1020.424079	62.59750144	785.3128553	67.23077833	1119.708584	67.92025406	781.176001	162.1646915
1.5	0	65.45882571	0	0	0	0	0	0	0	0	0	0
Averages												
0.3 (m)	1629.231148	203.349375	0	0	0	0	1713.577012	189.1002099	1918.121478	196.247775	1409.977866	130.1040701
0.6 (m)	1409.518215	145.134641	1409.28839	180.9873789	0	0	1741.270954	199.6491886	2112.323808	175.3566604	1409.748041	96.04396905
1.5 (m)	1145.678836	91.68475875	1183.370176	116.6133283	1024.331108	92.22657176	804.1585253	78.41867116	1065.929477	105.1289609	773.8215932	90.66605836

Figure 9.11 Pressure values calculated by DAS computer in kPa

APPENDIX I

PICTURES

Pictures of each barrier after testing was completed.

Solid concrete barrier



Barrier with cavity no LCFs



Barrier with cavity and LCFs



Barrier with foam



Barrier with pumice



Barrier with steel grit



BIBLIOGRAPHY

Brewer, Judy. 1999. *Scientific Principles*. [Online] c/o MAST Modules, Department of Materials Science and Engineering University of Illinois (UIUC), 1999. <http://matse1.matse.illinois.edu/concrete/prin.html>.

Brewer, Judy. 1999. *The Basic Mix*. [Online] c/o MAST Modules, Department of Materials Science and Engineering University of Illinois (UIUC), 1999. <http://matse1.matse.illinois.edu/concrete/bm.html>.

Ductal[®] – an ultra-high performance material for resistance to blasts and impacts. Cavill B; Rebentrost M. and Perry V. 2006. 1st Specialty Conference on Disaster Mitigation. Calgary, Alberta, Canada. May 23-26, 2006.

MODELING AND SIMULATION OF BLAST WAVE FOR PRESSURE SENSOR DESIGN. B.S. Chaurasia, S. Tandon, S. Shukla, P. Mishra, Anand Mohan and S.K. Balasubramanian. May 2011. International Journal of Advances in Engineering & Technology, ISSN: 2231-1963.

Cooper, Paul W. 1996. *Explosives Engineering*. s.l. : Wiley-VCH, 1996.

Daraio C; Nesterenko V.F.; Herbold E.B. and Jin S. *Energy trapping and shock disintegration in a composite granular medium*. Materials Science and Engineering Program, Department of Mechanical and Aerospace Engineering. University of California at San Diego, La Jolla. [Print].

ProPerma Engineered Coatings. Jan 2014. 4 Oct. 2014. <http://www.properma.com/products/lcfr>.

Pumice as a Sympathetic Detonation Barrier. Koontz, Bob and Cykowski, Ed. 1999. 1999. INSENSITIVE MUNITIONS AND ENERGETIC MATERIALS TECHNOLOGY SYMPOSIUM; 299-304.

Shock (Blast) Mitigation by “Soft” Condensed Matter. Nesterenko F, Vitali. 2003. 2003. MRS Symp. Proc., vol. 759 (MRS, Pittsburgh, PA, 2003), pp. MM4.3.1-4.3.12.

Predicting the effectiveness of blast wall barriers using neural networks. Remennikov M, Alex. and Rose A, Timothy. 27 March 2007. 2007, International Journal of Impact Engineering, 34 (2007) pp. 1907-1923.

MATLAB 2012a, The MathWorks, Inc., Natick, Massachusetts, United States.

Rouse Thomas, Nathan. *The Mitigation Effects of a Barrier Wall on Blast Wave Pressures*. MS thesis. Missouri University of Science and Technology. Rolla. 2010. [Print].

Swisdak Michael, M Jr.: Ward Jerry, M. *DDESB Blast Effects Computer, Version 5.0, User's Manual An Documentation*. Department of Defense Explosives Safety Board, Alexandria Virginia. [Print]. 1 May 2003.

Tinsley Matthew. Myers J, John. *Investigation of a High-Volume Fly Ash-Wood Fiber Material subjected to Low-Velocity Impact and Blast Loads*. University Missouri Rolla, Rolla. [Print].

Prediction of airblast loads on structures behind a protective barrier. Zhou, X.Q. and Hao, H. 27 March 2007. 2007, International Journal of Impact Engineering, 35 (2008) pp. 363-375.

Jeffery S. Volz, Jason Baird, Andrea J. Schokker, Eric S. Musselman, "“Long” Carbon Fibers for Blast Resistant Concrete," (2010) Final Rept., Leonard Wood Institute Research Program.

VITA

Caleb M Baumgart was born in Kansas City, Missouri. In May of 2009 he received his B.S. in Aerospace Engineering from the Missouri University of Science and Technology, Rolla, Missouri. He did his summer training at EaglePicher, Joplin, Missouri in the summer of 2011. In December 2013 he achieved an M.S. degree in Mechanical Engineering from the Missouri University of Science and Technology, Rolla, Missouri. In December 2014 he received his M.S. in Explosives Engineering from the Missouri University of Science and Technology, Rolla, Missouri.

He has been a student member of the international society of explosive engineers since 2011. He is a lifetime member of the Pyrotechnics Guild International since 2012.